LIBRARY
Michigan State
University

MICHIGAN STATE LIBRARIES
3 1293 01787 9945

This is to certify that the

thesis entitled

PREDICTING SOIL WATER CONTENT FROM TOPOGRAPHIC WETNESS INDICES IN LOW RELIEF TERRAIN: VALIDATION AND EVALUATION

presented by

DEMETRIOS GATZIOLIS

has been accepted towards fulfillment
of the requirements for

MASTERS OF SCIENCE degree in FORESTRY

Major professor

Date 12/14/98

O-7639

MSU is an Affirmative Action/Equal Opportunity Institution

PLACE IN RETURN BOX to remove this checkout from your record.
TO AVOID FINES return on or before date due.
MAY BE RECALLED with earlier due date if requested.

DATE DUE	DATE DUE	DATE DUE
OCT 01 2002		

1/98 c/CIRC/DateDue.p65-p.14

PREDICTING SOIL WATER CONTENT FROM TOPOGRAPHIC WETNESS INDICES IN LOW-RELIEF TERRAIN: VALIDATION AND EVALUATION

By

Demetrios Gatziolis

A THESIS

Submitted to
Michigan State University
in partial fulfillement of the requirements
for the degree of

MASTER OF SCIENCE

Department of Forestry

1999

ABSTRACT

PREDICTING SOIL WATER CONTENT FROM TOPOGRAPHIC WETNESS INDICES IN LOW-RELIEF TERRAIN: VALIDATION AND EVALUATION

By

Demetrios Gatziolis

The handful of spatially distributed, terrain-based indices of soil water content developed to date suggest the potential for characterizing a critical environmental variable at a fine spatial scale using widely available, inexpensive digital elevation and soils data. However, none of these indices have been validated against field observations of soil water content. The performance of static and dynamic indices in representing field observations of soil water content was evaluated for a 265 hectare, midwestern U.S. watershed, using publicly available data on soil attributes and elevation, and a terrain representation constructed via softcopy photogrammetry. Performance tests spanned a wide range of observed soil water content, and several agricultural and forest cover conditions. Contrary to expectation, all indices explained only a limited portion of the observed variability in soil water content. Changes in model structure which could improve index performance will likely sacrifice structural simplicity and parsimonious parameterization. Specific suggestions for alterations likely to improve model performance are presented.

To my benefactor,

Professor George Bouyoukos

ACKNOWLEDGMENTS

I would like to acknowledge the following individuals, organizations, and companies for their contributions to the success of this thesis: John Suppnick at the Michigan Department of Environmental Quality; Patrick Lindemann, Ingham County Drain Commissioner; John Gallant at the Australian National University, Camberra, Australia; the farmers of Barnard Drain who provided unrestricted access to their land; Kucera International Inc., for the set of aerial photographs; James Hart and Phu Nguyen for assistance with the soil sampling and Carl Ramm for his help with "the quantification of the obvious", all at the Department of Forestry at Michigan State University; and Professors Spyridon Dafis, Evangelos Sfakiotakis, and Spyridon Sakellariadis at the Aristotle University of Thessaloniki, Greece, for selecting me as recipient of the George Bouyoukos fellowship. I am grateful to Mark Zweifler for his assistance and eagerness to share with me portions of the spatial dataset.

I would especially like to thank Jeremy Fried, my advisor, for his guidance, encouragement, and continuous support along the progress of this thesis and during my medical misfortune. I also thank Daniel Brown and Jianquo Liu, the other members of my committee, for their valuable contributions.

Finally, I feel indebted to the late Professor George Bouyoukos, my benefactor, who with his fellowship and perspicacity provided me with the opportunity to convert participation in a graduate program from a dream to reality.

TABLE OF CONTENTS

LIST OF TABLES

LIST OF FIGURES

Key to Abbreviations

Abbreviation	Text
AML	Arc/Info Macro Language
ANOVA	Analysis of Variance
Arc/Info	GIS software used
DEM	Digital Elevation Model
DEM/P	10-m photogrammetrically-generated Digital Elevation Model
DEM/T	10-m Digital Elevation Model generated from contour-line interpolation
DEMON	Digital Elevation Model Networks
DLG	Digital Line Graph
DTM	Digital Terrain Model
DWI	Dynamic Wetness Index
DYNWETG	Dynamic Wetness (program) - GRID version
GIS	Geographic Information Systems
GPS	Global Positioning System
LDD	Local Drainage Direction
MSU	Michigan State University
SWI	Static Wetness Index
TAPESG	Terrain Analysis Programs for the Environmental Sciences - GRID version
TDR	Time Domain Reflectometry
TIN	Triangulated Irregular Network

Key to Abbreviations (cont'd).

TWI	Topographic Wetness Index
USDA-NRCS	United States Department of Agriculture - National Resource Conservation Service
USGS	United States Geological Survey

Key to variable declarations and descriptions

Variable	Description
A_{CIT}	Channel initiation area
A_e	Effective upslope contributing area
A_s	Specific upslope contributing area
δ	Dynamic wetness index
$\delta_{\%}$	Ordinal (percentile) transform of δ
$\delta_{\%20}$	Area defined 20%-ile of δ
δ_p	Plot δ, a 9-cell mean
ϕ_s	Spearman's rank correlation probability
K	Saturated hydraulic conductivity (mm/h)
λ	Observed soil water content (m^3 / m^3)
M_{im}	51 x 22 element matrix of observed soil water content (I = Plot vector, M = Sampling round)
P	Drainable porosity (m^3 / m^3)
PR_{ijk}	51 x 4 x 124 three-dimensional matrix of simulated soil water content (I = Plot vector, j = DEM choice, soil property assumption, k = drainage time)
τ	Drainage time (hours)
$\tan\beta$	Slope
τ_{As}	τ for which $A_e = A_s$ for all locations off of the drainage network
τ_{gc}	τ for which $A_e < 100m^2$
τ_{kc1}	Min τ for which equal δ and λ value distribution kurtosis coefficients are observed

Key to variable declarations and descriptions (cont'd).

τ_{kc2}	Max τ for which equal δ and λ value distribution kurtosis coefficients are observed
ν	Scaling exponent for A_s
ζ	Static wetness index
$\zeta_{\%}$	Ordinal (percentile) transform of ζ
$\zeta_{\%D}$	$\zeta_{\%}$ computed using the DEMON flow routing algorithm
ζ_{sc}	$\ln(A_s^{\nu} / \tan\beta)$

INTRODUCTION

The classical model of hillslope hydrology, based on infiltration theory (Horton, 1933), represents the first published report of an attempt to portray the downslope movement of runoff in a spatially explicit fashion. A re-examination of the simplistic assumptions embedded in this model led to modifications (Hillel, 1971) which ultimately produced a more realistic, but increasingly complex series of lumped- and distributed-parameter models (Beven and Kirkby, 1979; O'Loughlin, 1986; Vertessy et al., 1990; Dietrich et al., 1993).

In lumped-parameter hydrological models, the sub-watershed forms the fundamental analysis unit, and a single value is calculated for the attributes of interest for a single location within this unit. In distributed-parameter models, the continuously variable sub-watershed entity is discretized via tessellation into internally homogenous areal elements, usually square grid cells, which are typically represented in a raster data model. Each element is described individually by a set of differential mass-balance equations referencing the inputs of distributed components, such as precipitation and atmospheric deposition, and contributions from adjacent elements (cells). These equations for all elements in the sub-watershed are then solved simultaneously over a small computational time element Δt.

The specific distinction between the two model types is that the lumped-parameter models predict attributes at a single location (usually the watershed outlet) while distributed parameter models generate attribute values for each cell. Consequently, distributed parameter models are more demanding of data storage and require input at a far greater resolution. The distributed-parameter structure is designed to account for spatial variability in watershed attributes (e.g., slopes, soils, vegetation) and the effects of this variability on modeled outputs, making it well-suited to analysis of heterogenous watersheds. The advent of geographic information systems (GIS) and increasingly powerful computational capabilities and storage capacity have facilitated the development of increasingly complex distributed-parameter models (Table 1).

Hydrological models can be further classified as to whether they are temporally discrete or continuous (Table 1). Discrete event models simulate the response of a watershed to a specific precipitation event, and require specification of the storm parameters (e.g., intensity, duration, and distribution). Continuous, clock-driven models often require specification of considerable additional meteorological and other parameters, including detailed information on soils, precipitation, and solar radiation in order to account for such processes as available water surface storage, snow accumulation, evapotranspiration, soil water content, runoff, infiltration rates, lateral soil water movement, pollutant accumulation, and erosion (Novotny and Olem, 1994).

Most hydrological index-based models do not provide a true accounting for water flow from one location to another in three-dimensional (or even two-dimensional) space. Rather, they assess the hydrologic response for each location based on the value(s) of calculated topographic indices such that locations with equivalent index values are assumed to exhibit the same local hydrological behavior regardless of watershed position.

The most widely used topographical index in hydrological simulations is $ln(A_s / tan\beta)$ where A_s is the specific area (sometimes referred to as upslope contributing area), or the area drained per unit contour length (or its raster approximation), and $tan\beta$ is the local slope (Moore et al., 1991; Quinn et al., 1995). The index value is greater for locations that receive runoff from large, upslope areas or are relatively flat. Theoretically, soils at locations with high watershed-relative index values have relatively greater water content content and are more likely to reach saturation during rain and snowmelt events. The index assumes that the watershed has reached a steady state drainage condition with each location receiving water from its entire upslope contributing area.

Topographic Wetness Indices (TWIs), such as $ln(A_s / tan\beta)$, (also known as Static Wetness Index [SWI]), are usually computed from either Digital Terrain Models (DTM) which represent elevation at irregularly spaced intervals or Digital Elevation Models (DEMs), which represent elevation on a regular grid (raster). DEMs are usually derived from digitized contour lines of existing topographic sheets or, more recently, directly from automated processing of stereo aerial/satellite data through digital image correlation techniques (Krzystek and Ackermann, 1995; Kolbl, 1996). In contour-line based DEMs the fidelity of the resulting terrain representation is driven by the contour density (Gao, 1997), the contour interval to DEM resolution ratio, and the interpolation algorithm employed (Carrara et al., 1997). Terrain attributes used in the calculation of TWIs are derived from directional derivatives of the land surface represented by the elevation model; hence choices of representation (e.g. data model and scale) are expected to have a substantial influence on the accuracy of the index. The two most influential terrain variables are roughness (local variability in elevation) and magnitude of relief. DEM-extracted terrain attribute quality deteriorates as slope decreases, especially below the 5% margin (Hammer et al., 1995). Roughness is closely related to the scale of the representation. Coarse scale representations of terrain entail reduced information content, result in a smoother-appearing landscape, and degrade the accuracy of terrain parameters, including flow length and slope (which tend to be underestimated) and ultimately, TWIs. Distribution of SWI value at different grid sizes showed that as the grid resolution becomes coarser, the percentage of high index values increases (Quinn et al., 1991; Vieux, 1993). Because accuracy can also be impaired by excessively fine scale representations (because of heightened sensitivity to errors in elevation), the chosen terrain representation scale (DEM resolution) should be comparable to terrain roughness. Topographic parameters computed for two study areas with moderate to steep relief in the western United States were shown to be significantly affected by the DEM resolution. A 10-m grid provided a substantial improvement in the quality of calculated topographic indices and hydrographs over coarser spacing (30 to 90 m), while very fine resolution (2 to 4 m) provided only marginal additional improvement (Zhang and Montgomery, 1994).

Watershed size also affects the distribution of TWI. Investigations over a wide range of watershed sizes determined that variability in SWI distribution moments is high in small watersheds (0.1 to 1 Km^2), where $tan\beta$ and A_s are comparably influential on SWI, and minimal in large ones (1 to 100 Km^2) (Wolock, 1995). In large watersheds, A_s becomes the primary SWI controlling parameter, but its progressively increasing value encountered for areas on or along the converging drainage network and towards the watershed outlet, offers only a marginal increase to the natural logarithm based index value for these areas.

SWI can also be affected by the choice of the algorithms applied to raster models of elevation to calculate flow direction in the computation of A_s. The single flow direction (deterministic 8-node, also known as D8), algorithm assumes that the contour length used in computing the specific area A_s is given by the grid cell size. According to this method all flow accumulated upslope of and from a given cell drains to only one of eight neighboring cells - the one with the steepest descent (O'Callaghan and Mark, 1984). The lack of realism in the topographic index maps generated by D8, lead to the development of Rho8 (Random 8-node) (Fairfield and Leymaire, 1991). Rho8 introduces a stochastic component in the D8's flow direction determination in which the expected value of a cell's flow direction is determined by aspect. Further refinements produced the FD8 and FRho8 algorithms, which allow flow divergence (i.e., routing flow to more than one cell). The FRho8 option produces more realistic delineation of contributing areas and eliminates parallel flow paths (a troublesome artifact of D8) (Quinn et al., 1991; Moore at al., 1993). Costa-Cabral and Burges (1994) proposed Digital Elevation Model Networks (DEMON) as the next iterative improvement, though the complexity of this approach and the apparent comparative realism of its output, make this contribution more revolutionary than evolutionary. Using a stream tube approach, DEMON–calculated flow paths width remains constant over planar terrain, and increases/decreases over divergent/convergent topography. These characteristics are quite attractive for modeling areas with gentle topography. The multiple flow direction algorithms (FD8, FRho8, and DEMON) all use two dimensional flow routing, are suitable for computing the A_s in TWIs, and represent significant improvements over the traditional D8 method (Moore, 1993). Combinations of flow direction algorithms, where algorithm selection is conditioned by local terrain, have emerged in hydrological modeling software packages (e.g., TAPESG [Moore and Gallant, 1997]). Algorithms permitting flow divergence are used in the watershed's channel initiation zone and until flow accumulation reaches a user defined threshold, to be substituted thereafter by strictly flow-convergent algorithms that better correspond to well defined drainage networks.

The $ln(A_s / tan\beta)$ index is commonly known as the wetness index because of its strong correlation with the distribution of soil water content (Moore et al., 1988). Linear combinations of the index with other terrain attributes were shown to be correlated to hydrological parameters (water table depth, slope, and discharge). Burt and Butcher (1986), report that the product of the wetness index and plan curvature gave the best correlation with soil water content potential, as compared to single parameter alternatives.

Although topography is a dominant factor in describing water flows in soils on steep slopes, other factors may become relatively more important in watersheds with low topographic relief. Soil properties control the subsurface soil drainage speed and thereby influence the spatial distribution of soil water content. Barling et al. (1994), developed a quasi-dynamic wetness index (DWI), calculated as $ln(A_e / tan\beta)$ to simulate soil water content in such terrain. This index relaxes the steady state assumption of the static ($ln(A_s / tan\beta)$) approach and accounts for the time it takes for water to redistribute following a rainfall event, ultimately yielding a potentially more accurate representation of soil water content patterns compared with the static wetness index. The dynamic index uses the effective upslope contributing area A_e instead of A_s, calculated for a user-specified drainage time. DWI considers water flow accumulation over a short (typically much shorter than for SWI) upslope distance, so even small errors in terrain representation can lead to gross errors in flow routing and index value, particularly for locations away from the primary drainage network and when D8 algorithm is used to route flow.

A number of models designed to describe a watershed's hydrologic regime combine SWI with other parameters that affect soil water content distribution (vegetation, solar radiation, evapotranspiration). Among these are one, based on a modified version of SWI, which accounts for the spatial distribution of evapotranspiration (Famiglietti and Wood, 1995), a SWI-TOPMODEL based attempt to delineate locations within the Elbe watershed likely to experience limited water availability (Muller-Wohlfeil et al., 1996), one which incorporates SWI into a riparian non-point source pollution remediation application (Fried et al., 1999), and one that uses TAPESC, SWI, and a canopy rainfall interception model for soil water content modeling in humid mountainous landscapes for which calibration with field measurements of soil water content yielded moderate model performance (Yeakley et al, 1999).

In essence, DWI extends SWI by adding a temporal dimension in the form of a drainage time parameter. DWI provides a range of possible soil water content conditions for the same location and has the potential of providing a better fit to seasonal and weather induced changes in the hydrologic regime of a watershed. Apart from the initial work of Barling et al, 1994, the authors are not aware of any other attempts to investigate this potential.

Undoubtedly, GIS software, digital databases, and environmental models offer new opportunities for the collection, storage, analysis, and display of spatially distributed biophysical data (Goodchild et al., 1996). However, in the rush to embrace the new technology, ground-truthing has received inadequate attention (Hammer et al., 1995), and there is a dearth of information regarding model validation. This study was undertaken to investigate the relationships between the wetness indices DWI and SWI and *in-situ* observations of surface soil water content with the objective of assessing the practical utility of these models for applications requiring such predictive power.

METHODS

This section contains three parts: 1) descriptions of the study area selection process, experimental design, and procedures used to collect field observations of soil water content; 2) an explanation of the modeling process, data sources, data structures, and guiding assumptions behind derivation of distributed topographic wetness; and 3) an outline of the statistical procedures used to assess wetness index validity. Additional detail on these topics can be found in appendices A-C.

Study Area

Three considerations influenced the choice of watershed for this analysis: model performance, logistics, and representativeness.

Model performance, as judged by the accuracy of soil water content representation, depends in part on the terrain attributes relief magnitude and roughness. Poor performance could be expected in watersheds that are almost entirely smooth and flat, and good performance in watersheds that are mostly rough and steep. Yet much of the agricultural land in the U.S., identified as the principal source of non-point sediment pollution (U.S. EPA, 1984), falls between these extremes, and for this kind of terrain, model performance has not been tested.

DWI (heretoforth denoted as δ) is determined by terrain and soil characteristics. Poor drainage conditions on agricultural land in southern Michigan led to the establishment of a drainage enhancement infrastructure, which included subterranean drainage tiles, beginning in the 1950s[1]. Drainage tiles are typically poorly documented and are often difficult to identify by observation, so it can be extremely difficult to establish their absence in any given area with certainty, especially for areas with high turnover in land tenure. Because drainage tiles can drastically alter soil hydrology in a manner not reflected in terrain models, watersheds otherwise suitable for model validation, were excluded if the status of subterranean drainage tiles could not be definitively established.

The need for frequent, repeated rounds of soil water content sampling and rapid access to the watershed within short time periods made proximity to Michigan State University an important selection criterion. Another was the cooperation of landowners in granting unrestricted access to soil water content monitoring sites, providing cultivated crop history, and leaving sampling plots relatively undisturbed. Finally, for our findings to be widely applicable (at least regionally), a watershed was sought containing terrain, soils, crops and tillage practices which could be considered representative of agricultural land in the midwestern U.S.

One watershed which meets these criteria is the 16.85 km^2 subwatershed of Sycamore Creek known as Barnard Drain (Figure 1), located just south of the city of Mason in Ingham County, Michigan approximately 30 km from MSU. Barnard Drain was constructed in the early 1960s to expedite the drainage of adjacent agricultural fields, and was cleared and widened in the late 1980s. The Ingham County Drain Commissioner has responsibility for its management and maintenance[2]. Percent slopes in this

[1] Personal communication with Patrick Lindemann, Ingham County Drain Commissioner, February 1997.
[2] Information provided by the Ingham County Drain Commissioner Office, March 1997.

subwatershed, as calculated via the finite differences algorithm[3] from a 10-m DEM (Figure 2) generated from a 1:24,000 USGS digital hypsography (contour line) coverage via Arc/Info's TOPOGRID algorithm (Hutchinson 1989), are very gentle (maximum 16.3, mean 2.5, and st.dev. 2.0). Geologic formations include till plains, moraines, and eskers (glacially deposited gravel and sand that form ridges 9 to 12 meters in height). Eskers, which are dominant in and adjacent to riparian areas, grade into moraines approximately one-half to one mile wide composed primarily of sandy loam soils that further grade into till planes with slopes of 6-18%. Organic soils can be found in depressions and along the drainage network. Common soil series include Capac and Colwood-Brookston loams and Marlette and Aubbeenaubbee-Capac sandy loams (Figure 3). Row crops and forests are the most common land use/cover (Table 2).

Twenty of the subwatershed's agricultural property owners and leaseholders agreed to provide access to land under their control and information on past and planned tillage practices and crop choices. All provided assurance that these lands were free of subterranean drainage control structures.

Timing of soil water content sampling

Choices concerning when to sample soil water content were constrained by considerations involving precipitation, temperature, and cropping characteristics. To make meaningful use of the "drainage time" parameter required by the δ model, some samples had to be collected when soil was at or near saturation. Soil water content could not be accurately measured when soil was frozen or too dry to permit insertion of the

[3] The finite differences algorithm estimates slope from the elevation change in the four cardinal directions

moisture probe. In the Sycamore Creek watershed, surface soil remains unfrozen from early April to late November, and mean monthly precipitation ranges from 58.2 to 92.5 millimeters during this period (Figure 27).

In fields where soybeans and corn are grown, evapotranspiration, a parameter not considered in the calculation of δ, becomes a significant influence on the soil water content regime by mid-July.

These considerations suggested two potential sampling periods: April to June, and September to November. However, the latter period appeared less favorable for two reasons: 1) the presence of mature crop plants would hinder relocation and re-measurement of sample plots, and 2) on average, there is less precipitation during these months (Figure 27) - not an encouraging prospect given that the relationship between TWI and soil water content is strongest in periods and areas with frequent rainfall (Troch et al., 1993; Barling et al., 1994). Thus, the April to June period was selected for water content sampling.

Soil water content sampling

Fifty-one locations were selected for establishment of soil water content sampling plots so as to represent the full spectrum of hydrologic conditions which occur in the Barnard Drain subwatershed. Parameters that influenced plot selection included upslope contributing area, slope, plan and profile curvature, soil type, proximity to the drainage network, crop, and presence/absence of tillage. The distribution of sample plots over the ranges of these parameters roughly reflects the area-weighted distribution of these parameters over the subwatershed (Tables 3 and 4). The suitability of candidate sites for plot establishment was judged using ocular estimates of the aforementioned parameters, with preference given to locations with high roughness.

The number of plots was constrained by the time required to complete a sampling round. Attempting to measure soil water content at too many locations could result in measurements being made at different drainage stages for a given sampling round and an increased probability of precipitation occuring between measurement of the first and last plots.

Soil properties are notorious for exhibiting high spatial variability (Vieira, 1981), and where tillage is used, they are likely to be even more heterogenous. Thus, a single water content measurement is not likely to be representative of the hydrologic regime over an area of any size. TWIs are usually implemented in raster, so each estimated wetness value effectively represents an area (one grid cell) rather than a zero-dimensional point. Collecting multiple soil water content measurements within a sampling plot which coincides with a grid cell provides a way to address scale and representational difficulties and should provide a more stable representation of the hydrologic regime on an areal basis. Measurement locations within each plot were established on a regular (systemmatic) grid as described below.

On each of the 51 sampling plots established for this study (and georeferenced with coordinates obtained using differential global positioning system to within +/- 2 m of true position), 9 measurement locations were established on a 3-meter grid (randomly oriented with respect to crop furrows, where present), to facilitate plot establishment and remeasurement and to enable the assessment of within-plot soil water content variability.

The systemmatic design proved a fortuitous choice when plot markings were lost (e.g., due to planting activity) and sampling locations within a plot had to be reestablished. Plots were established within a small area (2.3 Km^2) of agricultural and forested land (Figure 4) with the goal of limiting complications from local variations in rainfall intensity.

Soil water content was measured using a ThetaProbe, a device that relies on the relationship between water molecule concentration and the apparent soil dielectric constant to estimate volumetric soil water content. Periodic calibration was conducted to ensure consistency of measurements throughout the study. Detailed calibration information and operation principles can be found in Appendix B.

The nine observations per plot were averaged for each of the 22 sampling rounds conducted between April 11 and June 11, 1997, to produce mean soil water content estimates which could be assigned to the grid-cell that contains the plot. These values were organized in a 51 by 22 element matrix M (51 plots, 22 sampling rounds).

Directional variograms calculated for each sampling round provided an estimate of spatial autocorrelation for the observed soil water content, and an opportunity to investigate possible direction-specific drainage patterns within the sampling area. Analysis of variance (ANOVA) for the observed soil water content was used to assess the influence of land use/cover on soil moisture conditions. The observed soil water content mean and standard deviation among plots per sampling round were regressed against drainage duration (time elapsed between sampling and the last rainfall event) to assess possible relationship(s) between soil water content condition and drainage stage.

Precipitation and water-table monitoring

Two rain gages were installed in the sampling area (Figure 4) to monitor temporal and spatial patterns of precipitation. Three ground water table monitoring tubes were installed at approximately equal intervals between Barnard Drain and the drainage divide, primarily to provide confirmation of the absence of artificial drainage patterns (e.g., from subterranean drainage tiles). Readings from rain gages and ground water monitoring tubes were recorded daily to ensure accurate precipitation and water table estimates

GIS Database Development

Distributed parameter inputs to and outputs from the topographic wetness index models (TAPESG – Version 6.3, 1997 and DYNWETG – Version 2.2, 1997), were managed as grids in an Arc/Info version 7.1.2 (ESRI, 1997) GIS database. Required inputs were elevation and two soil properties: saturated hydraulic conductivity and drainable porosity.

Two elevation grids were generated and used in simulations; both were represented in the GIS as co-registered DEMs with a grid cell edge length of 10 m (the same dimension used to define field water content measurement plots). DEM/T (Figure 2), was generated by processing a digital line graph (DLG) file, of topographic contours (10 foot contour interval) for the hypsography layer in the Mason and Leslie, MI, 1:24,000 series topographic quadrangle map sheets[4], with Arc/Info's TOPOGRID module. The module was executed using recommended tolerances for sink removal with drainage enforcement to the Barnard Drain. An alternative version of DEM/T, constructed using an intermediate Triangulated Irregular Network (TIN) elevation structure, was also attempted, but proved inferior for purposes of this study (See Appendix A).

DEM/P (Figure 5) was created by processing 1:24,000 scale aerial photographs, taken from an approximate height of 2,900 m above the ground (Kucera International[5], May 1995, 203 x 203 mm diapositive film sheets) via PCI software's PPOINT, XPACE, and ORTHOENGINE modules (PCI, version 6.2, 1997)[6]. GPS-georeferenced road intersections for which elevation is displayed on USGS quads served as ground control points. Photographs were scanned at 300 and at 600 dpi (11.8 and 23.6dpmm) resolution; however, at 600 dpi, perhaps due to homogenous crop patterns across much of the study area, the DEM generating algorithms frequently failed to provide an elevation solution. The 300 dpi DEM contained a number of spurious peaks and sinks that were eliminated via manual editing and a sink-filling routine in Arc/Info's GRID module respectively.

Comparison of the extrema and first and second moments for elevation and slope derived from DEM/P and DEM/T revealed no significant differences (Table 5); however, differences in local roughness as represented by comparable statistics on neighborhood standard deviation were significant (Figure 6 and Table 6). The lack of locations with precisely known elevation in the study area precluded direct assessment of DEM accuracy; thus, indirect methods were used to evaluate DEM quality.

GPS-referenced locations where evidence of past surface erosion was observed always coincided with a 12-meter buffer constructed around the drainage network

---

[4] obtained from USGS

[5] Kucera International Inc., 38133 Western Parkway, Willoughby, Ohio 44094-7589

extracted from DEM/P using the DEMON algorithm in TAPESG. This was not the case for the drainage network extracted from DEM/T. Field comparisons of the sign of relative elevation difference (positive or negative) between each plot and its nearest neighboring plots[7] within a 100 meter radius were always in agreement with DEM/P reported elevation, but for only 79% of the 182 plot elevation comparisons in DEM/T.

The spatial distribution of SWI (heretoforth denoted as ζ) formed a basis for investigating elevation correspondence between the two DEMs. Because A_s varies by several orders of magnitude across the watershed (resulting in a very wide range of ζ values), a range independent proxy, $\zeta_{\%}$, was calculated by a percentile rescaling of ζ. Locations with $\zeta_{\%} > 95$ are likely to coincide with the drainage network (Figure 7). While the DEM/P and DEM/T based $\zeta_{\%}$ maps in Figure 7 imply a common delineation of Barnard Drain, there is no spatial correspondence in the depiction of ephemeral tributaries. The spatial distribution of δ values couldn't be used in the same context because when $\delta_{\%}$, the percentile transform of δ, exceeds 95 or even 90, the resulting stream "network" is discontinuous.

This outcome could well be an artifact of how the DEMs were constructed. While delineating the contour lines from which DEM/T was derived, the stereo-plotter operator would most likely have used Barnard Drain as an elevation reference to improve positional accuracy. The absence of patternless, homogenous areas of crops in the riparian corridor would probably have minimized the probability of pixel-matching error

[6] PCI, 50 West Wilmot St., Richmond Hill, Ontario, Canada, L4B 1M5
[7] Where more than one adjacent plots were within a short (approximately 10°) viewing azimuth, only the nearest was considered for the comparison.

in the solution of the stereo model used for the creation of DEM/P, thereby resulting in a more accurate representation of terrain near Barnard Drain.

While positional discrepancies in the delineation of ephemeral tributaries (defined by $\zeta_{\%} > 95$) could be a result of differences in local roughness between the two DEMs which influence the form of the local drainage direction (LDD) network, the distribution of A_s, and ultimately, the distribution of ζ, this explanation is not as plausible as one based on errors in terrain representation with greater magnitude than local roughness. A frequency distribution of the elevation difference between the DEMs displays abrupt peaks (Figure 8) reflecting the distinctive stair-step elevation pattern in DEM/T long known to be associated with automated interpolation from contour lines (Eklundh and Martensson, 1995). Such "flat terraces" along contour lines could well introduce errors in the LDD network, particularly at locations both close to contour lines and situated downslope from the channel initialization zone. D8, a flow-routing algorithm incapable of representing dispersion, has been shown to perform poorly under these conditions (Band, 1989).

Collectively, these findings and considerations make DEM/P a superior choice for terrain representation. However, the absolute accuracy of DEM/P could not be determined so errors in the terrain model could still exert an unpredictable influence on terrain indices derived from elevation.

Saturated hydraulic conductivity (K) and effective porosity (P), parameters required for the calculation of δ, are both spatially heterogeneous and difficult to obtain (Iorgulescu and Jordan, 1994). Uniform, area-weighted average values for these parameters and distributed raster representations were estimated from surrogate measures in the USDA NRCS Ingham County Soil Survey digital database associated with the digitized version of the county soil survey map. Permeability, the rate of vertical movement of water through a soil column in inches/hour measured in laboratory environment, served as a surrogate for K. Specifically, the weighted-by-horizon-thickness mean permeability for all surface soil horizons was used as a proxy for K. Because soil water distribution during the drainage process is dominated primarily by near-surface flows, only surface soil horizons were considered. Surface horizons were identified as those stratified above the high water table and above a fine texture horizon with minimal permeability (less than $0.353*10^{-6}$ m / s). Drainable porosity, estimated from soil texture class and a table relating texture classifications to drainable porosity (Foth 1984, Figure 3-12), was used as a surrogate for P. Where the surrogate parameter value was available as a range the median value was selected (Fried et al., 1999). Drainable porosity and hydraulic conductivity were stored as grids co-registered with the DEMs.

Generation of TWIs

DEM/T and DEM/P were each processed with TAPESG to produce estimates of slope and local drainage direction, which were then processed by DYNWETG to compute rasters of δ for both uniform and distributed soil parameter options for a wide range of drainage times spanning 100 – 1,000,000 hours, and ζ (The drainage time parameter [heretoforth denoted as τ] is a driving variable which helps determine the extent of A_e). Thus, a total of six sets of TWI Models were generated: 1) DEM/T Dynamic Uniform Soils, 2) DEM/T Dynamic Variable Soils, 3) DEM/P Dynamic

Uniform Soils, 4) DEM/P Dynamic Variable Soils, 5) DEM/T Static and, 6) DEM/P Static. The distributed Wetness Indices were transferred to Arc/Info grid files using a conversion routine in the TAPES package (TAPESTOARC), and were processed with a 3x3-cell low pass filter to ensure better spatial correspondence between modeled wetness values and observed soil water content (given potential errors in registration of sample plot locations). The wetness index value for each grid cell containing a sampling plot and per simulation was extracted from the grid files and organized in a 51 by 4 by 124 matrix PR (51 plots, 4 DEM/soil property combinations, and 124 τ's; 123 in the 100 – 1,000,000 hours range plus the static [infinite τ]). Further details can be found in Appendix C.

Statistical Analysis

The performance of terrain based indices of soil water content was evaluated through the degree of association between model predicted index values and observed values of soil water content. Spearman's Rho, a non-parametric rank correlation statistic, was used to evaluate model performance because the distribution of index values is considerably affected by the drainage time specified, the sensitivity of observed water content to drainage stage, and the lack of normality in both predicted and observed soil water content distributions (see results section). Because Spearman's Rho utilizes attribute value ranking to assess variable correlation, it requires no assumptions about the distributional form (McClave and Benson, 1991; SPSS, 1997).

Spearman's correlation coefficients were calculated for each model and sampling day-- i.e., all combinations of PR_{ijk} and M_{im} where i represents plot ID (1-51), j references model assumptions (e.g., DEM choice, treatment of soil properties), k references drainage time parameter, and m represents sampling round (Figure 9). The resulting Spearman's Rho values, for each DEM-type and uniform/variable soil attribute combination, were plotted against τ to investigate model sensitivity to a) τ, b) soil attribute treatment, and c) DEM derivation technique.

RESULTS

This section contains three parts: 1) analysis of observed soil water content (λ) and related parameters, 2) analysis of predicted soil water content and related parameters, and 3) statistical evaluation of correspondence between λ and TWI.

Analysis of the observed soil water content and related parameters

Both topographic wetness indices used as proxies for soil water content are limited by the simplifying assumption of constant values for such attributes as land use/cover, evapotranspiration and precipitation. In fact, these may well vary within the sampled space and exert profound influences on λ (Barling et al., 1994).

Precipitation recorded by two, widely separated rain gages in the study area during the sampling period (Figure 10) was statistically identical (χ^2 test showed $p > 0.999$). Crop vegetation was absent for the first half of the sampling period and only seedlings were present by the end of the sampling period (maximum plant height < 12 cm), so differences in transpiration among most land use/cover conditions (except forest) were probably negligible. Solar radiation would also have varied little over the study area given its gentle terrain and narrow range of aspects represented (mostly north-east to south-east); thus, evaporation would likely have been relatively uniform. Data from the water table depth monitoring tubes (Figure 11) suggests that the water table rises for up to two days after a major (> 5 mm) precipitation event, followed by a slow drop, providing additional confirmation of the absence of artificial drainage.

Analysis of variance of soil water content for the 22 sampling rounds revealed a statistically significant ($p < 0.001$) land use/cover specific effect on λ (Table 7). The existence of somewhat higher significance ($p > 0.005$) for 3 out of 22 sampling rounds could be traced to incomplete representation of all five land use/cover conditions in those sampling rounds. Land cover classes in which tillage was present were drier that those without tillage; forested plots were wettest, perhaps because of their proximity to the Drain or reduced surface evaporation thanks to the influence of forest cover (Figure 12).

Variograms of λ (Figure 13), calculated for each sampling round, showed no evidence of directional anisotropy. Autocorrelation in λ was present to a distance (variogram range) of 450 meters. Variogram range variability between sampling rounds was negligible (minimum to maximum range difference was < 20m). The λ variability was always smaller (low variogram sill) for sampling rounds conducted at the beginning or end of a drainage stage (i.e., either immediately after or at least three days following major precipitation events) than those in the interim. To explore this relationship, λ was regressed on the drainage process duration (time elapsed since the last major [> 5 mm] precipitation event, rounded to the nearest half day). This regression ($R^2 = 0.864$) suggests a linear decrease in the soil water content with drainage process duration (Figure 14). Absence of detectable patterns in the plot of regression residuals by drainage process duration (Figure 15) supports the assumption that surface soil drying relates linearly to time.

A quadratic regression of the standard deviation of λ among all sampling plots on the drainage process duration was significant ($p = 0.006$), showing higher among-plot variability of λ for the second and third day of the drainage process and lower for all others (Figure 16).

Analysis of predicted soil water content

The grid of ζ for the study area calculated in Arc/Info GRID from A_s and $tan\beta$ derived from DEM/P via TAPESG/DEMON and finite difference algorithm, respectively exhibits a right-skewed frequency distribution with mean 9.01, minimum 5.51, and maximum 19.52 (Figure 17). An analogous grid calculated for the entire Barnard Drain subwatershed had mean, minimum and maximum values of 9.17, 5.51, and 22.60, respectively, a result consistent with Wolock's (1995) observation that the moments of ζ distribution exhibit stationarity for watersheds 1 Km^2 and larger. Corresponding DEM/T-based analysis results for ζ can be found at Figure 18.

The variety of input data choices available for each dimension in the PR matrix produce a j, k combination-specific value range for each δ_{jk} vector within PR, thus making a range independent δ value transformation necessary for effective interpretation and portrayal of the spatial distribution of δ. Thus $\delta_{\%20}$, an area defined 20%-ile ordinal transformation of δ was calculated. Very narrow (sometimes 0) ranges of δ caused by gentle relief and uniform soil attributes necessitated grouping adjacent $\delta_{\%20}$ classes for low values of τ.

Where uniform soil attributes are used, δ depends exclusively on terrain attributes, and assignment of grid cells to $\delta_{\%20}$ classes is determined by local slope for small τ and A_e for large τ (Figure 19). Compared to large values of τ (> 100,000), A_e is small and flow paths short for τ < 5,000 hours, effectively concealing the drainage network (Figure 19). When τ < 3,400 hours the range of δ values is on the order of 0.3% soil water content (Figure 20a); range increases rapidly until τ = 25,000 hours. τ = 3,400 hours marks the threshold (τ_{gc}) above which, for the average slope found in the sampling area, A_e can exceed the $100m^2$ (the area occupied by a single grid cell). τ = 25,000 hours corresponds to the maximum time (τ_{As}) needed for all locations off of the drainage network to achieve $A_e = A_s$. The presence of distributed soil attributes widens the range of δ for $\tau < \tau_{gc}$ (> 2% soil water content) (Figure 20b) and replaces slope as δ's controlling factor in such cases. Figure 21 illustrates the direct spatial correspondence between large drainable porosity (P) and membership in the upper $\delta_{\%20}$ class for small τ (5,000 hours), an artifact that is not observable for large τ (100,000 hours).

The shape of the curve that portrays the relationship of δ_p (plot δ, a 9 cell mean) and τ reveals the geomorphologic characteristics of the watershed along the flow path above the plot location. Curves which reach an early asymptote (ex. Sampling plot 3, Figure 20) typically represent locations proximal to local terrain maxima; continuously rising curves signal locations on the drainage network (Plot 1). In the absence of rugged terrain, curves featuring alternating sigmoid sections (Plot 28), suggest alternating areas of divergent and convergent flow upslope, especially when calculated for uniform soil attributes.

Figure 22 illustrates the combined impact of τ and uniform/distributed soil attributes on the δ value distribution calculated for DEM/P. For $\tau < \tau_{gc}$, the distribution's kurtosis coefficient is large (narrow distribution), and the discrepancy between the mean index value for uniform versus distributed soil attributes is noticeable. Even larger kurtosis coefficients would have been calculated if the algorithm used to calculate δ had been incapable of handling sub-cell A_e. As τ gradually increases, the distribution form shifts from leptokurtic to platokurtic with an abrupt reduction on the kurtosis coefficient observed when $\tau = \tau_{gc}$. The critical value is smaller for soil types that permit higher subsurface water redistribution velocities. Finally, for large τ the influence of soil attribute representation (i.e., distributed or uniform) on the mean index value becomes minimal.

Statistical analysis

Spearman's rank correlation probability (ϕ_s), calculated between PR_{ijk} and M_{im} ($\forall$ i, j, k, and m) and plotted against τ, showed low correspondence between predicted and observed soil water content (Figures 23 and 24). The rate of change in the calculated ϕ_s with τ exhibited consistent patterns among different sampling rounds for $\tau < \tau_{gc}$. Beyond that threshold, the uniform probability change rate among different sampling rounds disappeared. Watershed drainage stage, defined as days since last precipitation event, affected ϕ_s but in an inconsistent fashion. Sampling rounds in initial drainage stage (less than 2 days since last precipitation) were alternating with those in lateral stages (at least 3 days since last precipitation) when ordered by ϕ_s magnitude regardless of τ. For $\tau > \tau_{gc}$, ϕ_s

declined rapidly, and for τ between 11,000 and 40,000 hours, virtually no association could be detected between PR and M. For larger τ, the association improved for sampling rounds which took place either during the first half of the sampling period, or immediately (within a day) following a major (> 10mm) precipitation event. Soil attribute representation affected ϕ_s only for $\tau < 3{,}400$, because of the relatively stronger influence of terrain attributes for larger τ.

When τ is smaller than τ_{gc}, δ appears to be controlled by P. Unless roughness is great, δ increases linearly with τ, and δ_p rank remains unchanged. Therefore, ϕ_s for $\tau < \tau_{gc}$ reflects the association between observed plot water content and P, which being stationary, causes the formation of parallel curves when plotted against τ. For $\tau > \tau_{gc}$ δ is controlled primarily by terrain attributes, and δ_p rank changes considerably with increasing τ (Figure 20). However, such a terrain-induced δ_p value ranking is inconsistent with corresponding plot λ ranking. For $\tau > \tau_{As}$, δ keeps increasing only for plots in the proximity of the drainage network, which gradually populate the upper tail of δ_p rank. Nearly saturated surface soil for plots on and in the proximity of the drainage network, preserved by either snow-melt induced near-surface flow early in the sampling season, or from runoff after intense precipitation, probably served to maintain these plots in the upper ranks of λ, thereby resulting in artificially improved ϕ_s.

The dependence of λ on land cultivation practices (as shown by ANOVA analysis, Table 7) motivated the calculation of ϕ_s separately for tillage and no tillage conditions (Figure 25a-d). Forested land was excluded because it contained only six plots, too few to yield reliable rank correlation coefficients. With the exception of distributed soil attributes and tillage combination, where ϕ_s showed smaller range of variability among sampling rounds for small τ, all other input information combinations exhibited low overall and highly variable ϕ_s, possibly because of the smaller sample sizes. Observations made above concerning the effect of τ on δ's performance when information for all plots was considered, were also applicable here. There was no indication that the tillage which occurred in the middle of the sampling period generated any noticeable effect on the behavior of δ (Figure 25a,b).

The lack of model significance for all soil attributes, land conditions, and τ combinations, motivated investigation of the association between individual terrain attributes and λ. To this end, local slope extracted from DEM/P for each plot using the finite differences algorithm was regressed against λ. The resulting regression proved highly insignificant for all sampling rounds ($p > 0.3$), which is an indication that errors in DEM extracted slope for gentle terrain may very well contribute to the lack of strong relationships between PR and M.

Another regression of $\ln(A_s)$ and $\ln(A_e)$ on λ, showed that although A_s or A_e explained only a small portion of soil water content variability ($R^2 < 0.1$), their influence was significant when the watershed was in lateral drainage stage (at least 3-4 days without precipitation) (Table 8). Regression significance was weaker for smaller τ and absent when A_s was used instead of A_e, regardless of the algorithm used to compute A_s and the watershed's drainage stage.

DISCUSSION

The primary hypothesis underlying this study was that the previously reported moderate relationship between static wetness index and measured soil water content (Wilson, 1996) could be traced to the limitations of this index's embedded assumptions that a watershed's hydrologic condition is in dynamic equilibrium (steady state condition), and that the value and spatial variability of soil attributes don't matter. The ability of the static wetness index ζ to predict soil water content might be improved if watershed drainage stage were added as an explanatory variable, but such improvement would be external to ζ and impose considerable additional data demands to make use of the index in predictive modeling of soil water content. A corollary to the above hypothesis was that the inclusion of soil attributes and the user-specified drainage time parameter τ in the calculation of dynamic wetness index δ would produce an index much more closely related to observed soil water content λ. This hypothesis proved difficult to definitively accept or reject because both ζ and δ proved at best weakly related to λ, though the relationship, as assessed by Spearman rank correlation, was slightly less weak in the case of δ. This discussion explores the possible influence of input accuracy on model performance, offers some insights into the conceptual structure of the wetness indices tested, and proposes new indices for further investigation.

Influence of accuracy of terrain representation and soil attributes

DEMs derived via interpolation from digitized elevation contours or DLG files are the most commonly used representations of terrain for a variety of applications (Carrara et. al, 1997; Gao 1997). The U.S. Geological Survey, the primary provider of DEMs in the U.S., reports elevation accuracy standards for every DLG file and for the contours included on standard topographic quadrangle map series, but does not provide accuracy estimates for extracted DEMs. Most algorithms for interpolating raster tessellations of elevation from contour lines utilize linear or spline functions to estimate elevation values between contours. This approach tends to produce terraces (flat spots) along contours and uniform slopes between these terraces. In gentle terrain, where the horizontal distance between contours often greatly exceeds the resolution of the interpolated DEM, these algorithms produce smooth surfaces between the contour lines, which offer not even a hint of the micro-scale perturbations found in most terrain. Terrain derivatives like slope and curvature have been found to be highly unreliable when slope is less than 5% (Hammer et. al., 1995). As suggested by the mean slope values in Table 5, the majority of sampling locations in this study had slopes of less than 5%. In addition to the obvious direct impact of slope error on ζ and δ (for which the equations include $tan\beta$ in the denominator) is the more subtle impact of having most slope change near source map contours, and the consequent effects on plan curvature and flow routing. Field observations in the study area revealed that mild plan curvature (< 2%), extending to a distance of 30m, was sufficient to produce localized flow convergence, a condition not observable on the raster maps of flow accumulation derived from DEM/T, even when the

DEMON flow routing algorithm was used. Error propagation analysis has shown that derivative GIS layers like terrain indices which are based on differences between uncertain values (elevation, in the case of the first derivatives slope and aspect, for example) almost always contain substantially more error than the source layer. As the order of DEM derivatives increases (from 0 for elevation to 1 for slope, and on to 2 for curvature), error can increase at an astonishing rate. For terrain indices like wetness, this is compounded further by the aggregation of derived values that is embodied in the calculations for upslope contributing area. Such cascading of errors may explain the lack of correspondence between the observed and calculated drainage network for the lower portion of the study subwatershed (Figure 7).

These considerations suggest that the information content of contour line maps, even at a scale of 1:24,000 and with a contour interval of 3.05 m, may well be inadequate for generating valid soil water content indices in gentle terrain.

Photogrammetrically generated DEMs are free of any reliance on interpolation, but are comparatively difficult to obtain. Besides requiring pairs of aerial photographs, photogrammetric techniques require detailed camera calibration information, sophisticated and expensive software operated by experienced users, and several well-distributed and well-defined points within the area of interest for which elevation is known. In practice, as of the late 1990s, this combination of requirements is rarely satisfied, and most DEM users settle for contour interpolation.

Field observations for this study suggested the superiority of DEM/P over DEM/T, as illustrated in Figure 7, where cells with $\zeta_{\%} > 95$ as calculated via DEM/P corresponded closely with the ephemeral stream network constructed from GPS-georeferenced field observations. However, it is possible that the accuracy improvement offered by DEM/P is limited to areas with distinct light reflectance patterns (e.g., where there is evidence of past runoff or riparian forest). All spurious sinks and peaks that were eliminated with editing during DEM/P development were located within uniform, row crop fields, and away from the drainage network.

The spatial distribution of soil attributes used in this study was derived from USDA NRCS County Soil Survey series, where soil types are mapped as homogenous polygons with crisp boundaries. Transitions in soil properties, or between soil types, are far more likely to be gradual, as suggested in the guidelines for using STATSCO data (USDA, 1994). Moreover, existence of large, supposedly homogenous polygons is incompatible with the widely recognized high spatial variability of soil attributes (Vieira, 1981). Many applications ignore soil transmissivity parameters, such as K, an attribute used in calculating δ, because spatial distribution of soil transmissivity is seldom known and often is considered to be constant over the watershed (Iorgulescu and Jordan, 1994). Yet typically, K exhibits high spatial variability and it is difficult to measure (Campbell, 1994). When used in models, K is more likely to be assigned values that will yield reasonable model results than to reflect actual field conditions (Dorsey et al, 1990; Ahuja et al., 1993; Mohanty et. al., 1994).

The accuracy of soil attribute and terrain information used in this study is unknown. Detailed surveying and a dense network of soil sampling could provide the close estimates of ground-truth needed to permit such accuracy assessment, but only at exorbitant cost. Many others who have applied GIS in modeling report difficulties in generating reliable, location-specific estimates for key variables, a serious problem when model outputs are highly sensitive to small changes in the values of these input variables (e.g., De Roo et al., 1989; Brown et al., 1993). In this application, if ζ or δ are to be useful in predicting λ on an operational basis, it must be possible to calculate them using publicly available information of the kind used in this study. The rest of this discussion is based on the premise that adequate accuracy of model inputs has been achieved.

Influence of index structure

Although ζ is a natural-logarithm based index, its value distribution is skewed to the right (Figure 17). This lack of distribution symmetry emanates from the very large A_s of locations on the drainage network. For the 2.3 Km^2 study area, values of ζ for such locations are 3.5 times as large as for local elevation maxima. The observed water content was at most (following three days without precipitation) 1.9 times greater on the wettest plot than on the driest one and at least (one day after precipitation) 1.3 times greater. These scale differences between observed water content and predicted TWI necessitated the use of scale independent statistical methods (i.e., Spearman's Rho). The performance of ζ was expected to be inferior for sampling rounds with a small range in λ (early or lateral drainage stages) and better for those in intermediate drainage stages. However, calculated ϕ_s showed poor model performance (corresponding $p > 0.3$) regardless of the watershed's drainage stage.

Unlike ζ, the family of δ distributions generated using DEM/P for different drainage times (Figure 22), includes a subset of distributions calculated for τ between 6,000 (τ_{kc1}) and 11,000 hours (τ_{kc2}), for which the kurtosis coefficient approximates the coefficients of the per sampling round λ distributions. The τ_{kc1} to τ_{kc2} range is included within the τ_{gc} and τ_{As} interval (Figure 26). Its proper calculation requires all drainage stages to be represented within the sampling rounds because the drainage stage affects the distribution of λ. It is watershed specific because it is affected by the values of soil attributes and local slope. Higher values for K and slope variability shift τ_{As} to lower τ values, while small variability in P, leads to a rightward shift in τ_{kc1} and τ_{kc2}. It was believed that δ would be most successful as a predictor of soil water content for $\tau_{kc1} < \tau < \tau_{kc2}$ because of similar δ and λ distribution forms, as indicated by equal kurtosis coefficients, in that range. Surprisingly, calculated ϕ_s for that range showed δ to have the least predictive τ. A satisfactory explanation for this result has been elusive .

Barling et. al., the developers of δ, evaluated their model against predictions of the depth of a perched water table/soil depth ratio. Surface soil water content exhibits much higher spatial and temporal variability than surrogate variables related to water table depth, and thus may be less closely related to terrain attributes. Yet surface soil water content is likely to be of far more interest to potential adopters of wetness indices than such surrogates.

Although similar in topography and although all non-forested plots were in the crop growth initiation stage for most of the study, land use/cover conditions within the sampling area featured statistically different observed soil water content (Figure 12 and Table 7). One possible explanation is differences in organic matter content and cultivation-method-specific disturbance of upper soil horizons. Poor or complete absence of association between the observed water content and both A_e (Table 8) and slope suggests problems with terrain representation accuracy.

Potential for index improvement

The influence of flow routing algorithm on ζ was shown to be of importance for locations both below and above the channel initiation zone. Unfortunately, the effect of DEMON flow routing algorithm on δ cannot be assessed because the algorithm is not an option in DYNWETG and the module does not provide a vector or raster representation of A_e for a selected location within the watershed, even for the D8 option. If those two options were available, it would be useful to explore the use of λ as a substitute for δ, calculating A_e for each plot location via

$$A_e = e^{\delta} \tan \beta ,$$

and observe the shape of the delineated area and the corresponding τ. The A_e shape calculated with DEMON and D8, would permit assessment of relative performance of these algorithms and of an appropriate τ range for calculating δ. It could also provide a better estimate of the most suitable channel initialization threshold to use.

The ζ value range calculated for large watersheds (> 1 Km^2) is unrealistically wide as compared to the range of observed soil water content. In large watersheds, scaling of the calculated A_s would result in an index value distribution equivalent to those observed with field measurements, and would possibly contribute to the improvement of ζ performance. A modified version of ζ, defined as

$$\zeta_{sc} = ln\ (A_s^{\nu} / tan\beta),$$

where ν is an exponent set to 1 for A_s less than or equal to the channel initiation threshold area (A_{CIT}), and set proportional to the A_{CIT} / A_s ratio for A_s greater than A_{CIT}. The distribution of ζ_{sc} wold have a kurtosis coefficient that approximates those for the λ distributions. The factor ν could be defined empirically for a particular grid resolution and terrain roughness with validation efforts similar to the one described in this study.

CONCLUSIONS

Terrain based indices of soil water content have become increasingly popular and are either used as components of soil erosion and non-point source pollution models (Wilson, 1996) or independently (e.g., to calculate hydrographs and identify zones of soil saturation). However, their ability to produce reliable predictions of surface soil water content in gentle terrain appears doubtful, especially when terrain representation or soil attribute accuracy are uncertain. Terrain derivatives and spatially distributed soil attributes obtainable from publicly available sources and used for index calculation appear to be unsuited to gentle terrain, and this hindered efforts to validate wetness indices. In addition to the unrealistic index assumptions (e.g., continuous, uniform precipitation for prolonged time ranges, soil water content at field capacity), the restriction of soil water content monitoring to near-surface conditions (where environmental parameters and anthropogenically induced disturbance such as evapotranspiration and crop cultivation, not considered by the indices, is likely to have introduced a level of stochasticity in soil water content variability), further frustrated validation efforts. Although a variety of index parameter estimation choices were utilized in this study, the set of options was not exhaustive because of technical difficulties associated with their computation (i.e., the DEMON flow routing algorithm could not be used to calculate effective upslope contributing area without a substantial rewrite of the TAPES software). Observations on the computed index value distributions, believed to be only minimally influenced by input information accuracy, although speculative in nature, suggested that index structural simplicity and parsimonious parameterization may need to be sacrificed to obtain a wetness index with a closer relationship to observed soil water content.

Table 1. **Characteristics of commonly used hydrologic models.**

Model	Authors	Lumped parameter	Distributed parameter	Continuous event	Discrete event
AGNPS	Young et al., 1986		X*	X	X
ANSWERS	Beasley, 1996		X		X
ARM	Donigian and Davis, 1978	X		X	
CREAMS	Knisel, 1986	X		X	X
TAPES	Moore et al., 1988		X		X
TOPMODEL	Beven and Kirkby, 1979		X	X	
WEPP	Laflen et al., 1991	X		X	X

*Distributed parameter description, lumped parameter routing.

Table 2. **Land use/cover in the Barnard Drain subwatershed (NRCS/CES/CFSA, 1990).**

Landuse	Km^2	Percent of Watershed
Residential	0.85	5.0
Commercial / Industrial	0.63	3.8
Crops	11.33	67.3
Pasture / Feedlot	0.56	3.3
Wetlands	0.33	2.0
Forest	2.73	16.2
Water	0.01	0.0
Other	0.39	2.4
Total	16.84	100.0

Table 3. **Distribution of sampling plots by land use/cover class over the sampling area, estimated from rectified aerial photographs obtained in 1995 and field observations during spring 1997.**

Land Use/Cover	Number of Plots	Percentage of Plots	Percent of Land Use/Cover Area
Corn w/ Tillage	9	17.6	16.5
Soybeans w/ Tillage	12	23.5	21.5
Corn w/o Tillage	11	21.6	19.5
Soybeans w/o Tillage	13	25.5	27.5
Forest	6	11.8	12.5
Other			2.5
Total	51	100.0	100.0

Table 4. Plot frequency by soil type.

Soil Type	Number of Plots	Percentage of Plots	Percent of Land Use/Cover Area
Colwood - Brookston Loam	3	5.9	6.8
Houghton Mack	3	5.9	5.7
Brady Sandy Loam	3	5.9	7.1
Capac Loam	42	82.4	77.8
Other			2.6
Total	51	100.0	100.0

Soil types determined via interpretation of orthophoto based soil maps (SCS, 1979).

Table 5. Summary statistics for slope and elevation derived from DEM/P and DEM/T.

	Elevation (m)			
	Minimun	Maximum	Mean	St.dev.
DEM/P	290.0	311.4	299.2	4.9
DEM/T	286.9	311.5	300.7	5.1
	Percent Slope*			
	Minimun	Maximum	Mean	St.dev.
DEM/P	0.000	12.328	1.165	0.706
DEM/T	0.000	12.109	1.156	0.704

*calculated with the finite difference algorithm in TAPESG.

Table 6. **Minimum, maximum, and mean of standard deviation of elevation derived from DEM/P and DEM/T within 3x3, 5x5, and 7x7 cell square neighborhoods.**

	Neigborhood Radius (cells)	Neigborhood st.dev minimum (m)	Neigborhood st.dev maximum (m)	Neigborhood st.dev mean (m)
DEM/P	3	0.005	1.753	0.519
	5	0.051	1.942	0.679
	7	0.118	2.215	0.991
DEM/T	3	0.001	1.125	0.146
	5	0.003	1.174	0.217
	7	0.004	1.368	0.258

Table 7. **ANOVA of observed soil water content (λ) on land use/cover condition for each sampling day.**

Sampling Day		Sum of Squares	df	Mean Square	F	Sig.
11-Apr	Among Groups	0.177	4	0.0441	14.162	0
	Within Groups	0.143	46	0.0031		
	Total	0.320	50			
13-Apr	Among Groups	0.092	4	0.0229	19.984	0
	Within Groups	0.053	46	0.0011		
	Total	0.144	50			
15-Apr	Among Groups	0.144	4	0.0359	14.728	0
	Within Groups	0.110	45	0.0024		
	Total	0.253	49			
18-Apr	Among Groups	0.149	4	0.0374	14.365	0
	Within Groups	0.120	46	0.0026		
	Total	0.269	50			
22-Apr	Among Groups	0.115	4	0.0287	13.138	0
	Within Groups	0.101	46	0.0022		
	Total	0.216	50			
23-Apr	Among Groups	0.103	4	0.0258	13.675	0
	Within Groups	0.087	46	0.0019		
	Total	0.190	50			
26-Apr	Among Groups	0.067	4	0.0169	6.823	0
	Within Groups	0.059	24	0.0025		
	Total	0.127	28			
6-May	Among Groups	0.131	4	0.0328	14.948	0
	Within Groups	0.101	46	0.0022		
	Total	0.232	50			
7-May	Among Groups	0.137	4	0.0341	13.242	0
	Within Groups	0.119	46	0.0026		
	Total	0.255	50			
10-May	Among Groups	0.143	4	0.0359	13.186	0
	Within Groups	0.125	46	0.0027		
	Total	0.269	50			
12-May	Among Groups	0.153	4	0.0382	13.542	0
	Within Groups	0.130	46	0.0028		
	Total	0.283	50			
15-May	Among Groups	0.026	4	0.0066	2.853	0.05
	Within Groups	0.049	21	0.0023		
	Total	0.075	25			
16-May	Among Groups	0.102	4	0.0256	10.398	0
	Within Groups	0.113	46	0.0025		
	Total	0.215	50			

Table 7 (cont'd).

Sampling Day		Sum of Squares	df	Mean Square	F	Sig.
18-May	Among Groups	0.156	4	0.0391	13.918	0
	Within Groups	0.129	46	0.0028		
	Total	0.285	50			
20-May	Among Groups	0.170	4	0.0426	18.124	0
	Within Groups	0.108	46	0.0024		
	Total	0.279	50			
22-May	Among Groups	0.219	4	0.0547	18.557	0
	Within Groups	0.135	46	0.0029		
	Total	0.354	50			
25-May	Among Groups	0.105	4	0.0263	16.526	0
	Within Groups	0.073	46	0.0016		
	Total	0.178	50			
27-May	Among Groups	0.190	4	0.0475	15.943	0
	Within Groups	0.137	46	0.0030		
	Total	0.327	50			
3-Jun	Among Groups	0.112	4	0.0281	12.239	0
	Within Groups	0.105	46	0.0023		
	Total	0.218	50			
6-Jun	Among Groups	0.063	4	0.0158	5.098	0
	Within Groups	0.099	32	0.0031		
	Total	0.162	36			
7-Jun	Among Groups	0.089	4	0.0223	6.549	0.01
	Within Groups	0.031	9	0.0034		
	Total	0.120	13			
11-Jun	Among Groups	0.017	4	0.0043	3.069	0.11
	Within Groups	0.008	6	0.0014		
	Total	0.026	10			

Table 8. R-squared coefficients for regression analysis of soil water content (λ) on DEM/P-derived A_e, calculated for three drainage times (τ), and A_s, calculated using the D8 and DEMON flow routing algorithms, using uniform and distributed soil attributes.

	A_e			A_s	
	τ (hours)				
	1,000	10,000	50,000	D8	DEMON
4/13[1]					
Uniform Attributes	0.0183	0.0268	0.0275	0.008	0.009
Distributed Attributes	0.0135	0.0141	0.0198		
4/23[2]					
Uniform Attributes	0.0523	0.0717*	0.0719*	0.000	0.038
Distributed Attributes	0.0471	0.0549*	0.0631*		
5/12[2]					
Uniform Attributes	0.0520	0.0905**	0.0772**	0.002	0.033
Distributed Attributes	0.0575*	0.0928**	0.0817**		

** Significance at the 0.1 level

** Significance at the 0.05 level

*[1] one day after precipitation

*[2] four days after precipitation

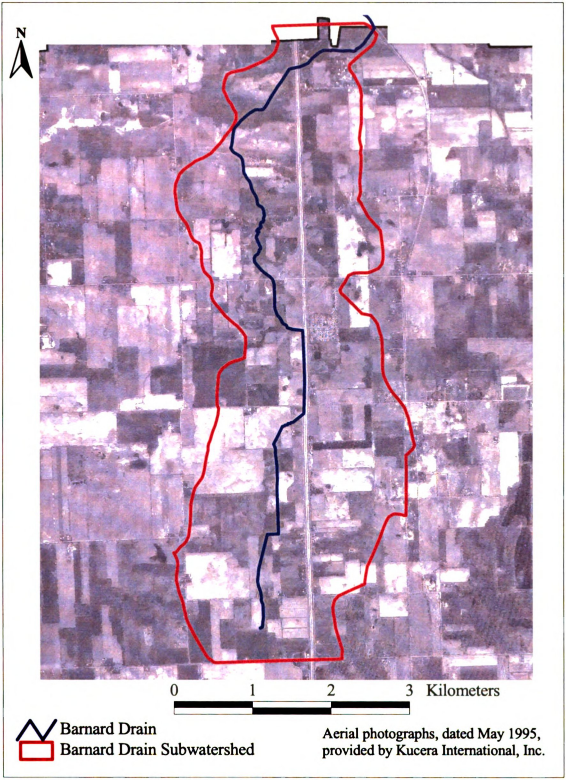

Figure 1. **Ortho-rectified aerial photograph mosaic of Barnard Drain subwatershed in Ingham County, Michigan. Study area is in the south-west third of the subwatershed.**

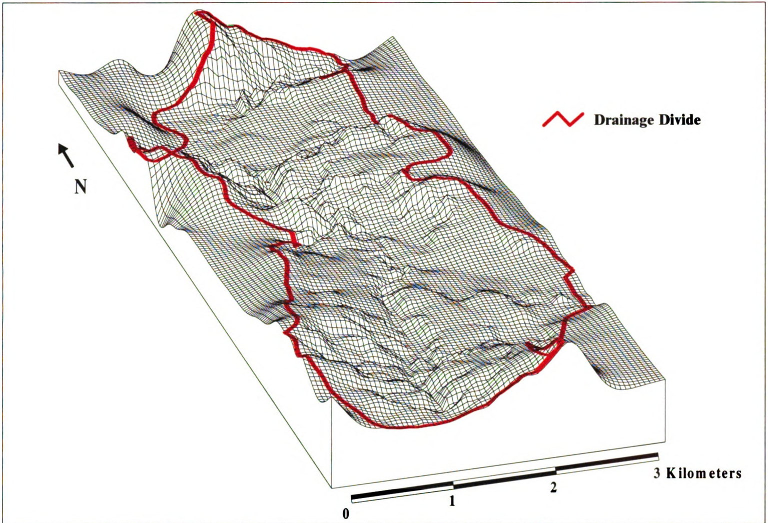

Figure 2. Surface drape of Barnard Drain subwatershed boundary on an elevation model derived from USGS 1:24,000 contour file using Arc/Info's TOPOGRID algorithm. Vertical exaggeration factor is 12.

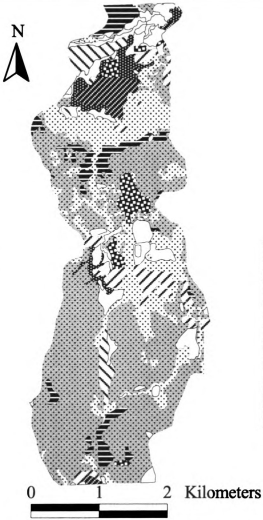

Soil Type	Drainable Porosity[1] (m^3/m^3)	Saturated Hydraulic Conductivity (mm/h)
Capac loam	0.26	33
Colwood-Brookston loam	0.28	33
Sebewa loam	0.26	36
Aubbeenaubbee-Capac sandy loam	0.34	94
Marlette fine sandy loam	0.30	102
Matherton sandy loam	0.34	64
Houghton muck	0.50	79
Udorthents and Udipsamments	0.34	76
Other	-	-

[1] Estimated from soil texture class and a table relating texture classifications to drainable porosity (Foth, 1984)

Figure 3. Soils in Barnard Drain subwatershed as defined in the 1979 Soil Survey of Ingham County, Michigan by USDA Soil Conservation Service.

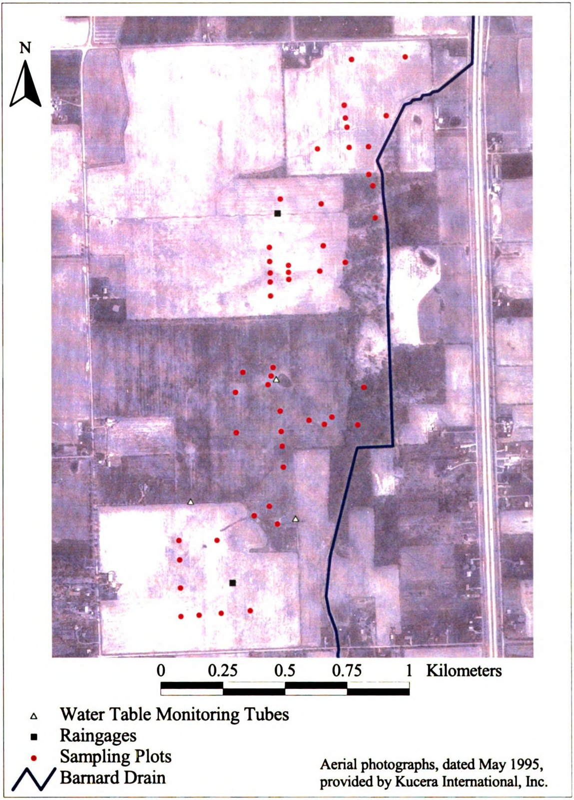

Figure 4. **Ortho-rectified aerial photograph mosaic of sampling plot allocation in the south-west third of Barnard Drain subwatershed in Ingham County, Michigan.**

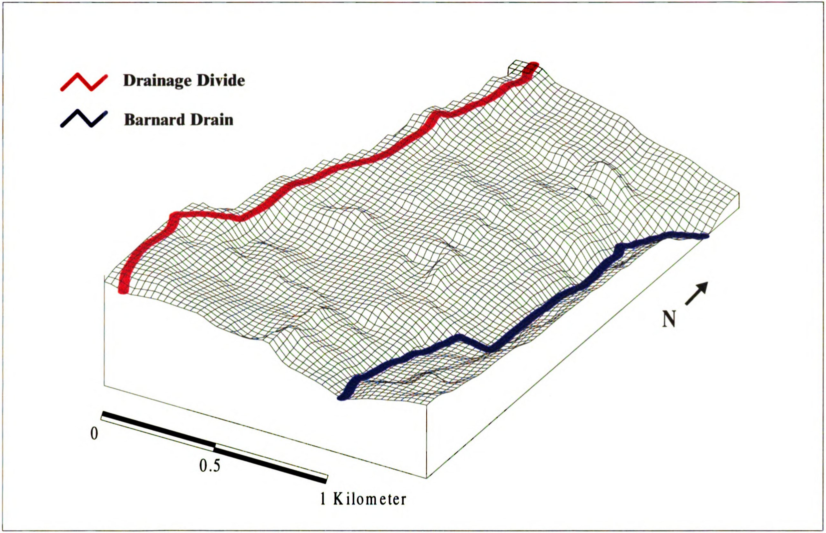

Figure 5. **Surface drape of the south-west third of Barnard Drain and its subwatershed boundary on an elevation model constructed from an aerial photography stereo pair using PCI software. Vertical exaggeration factor is 12.**

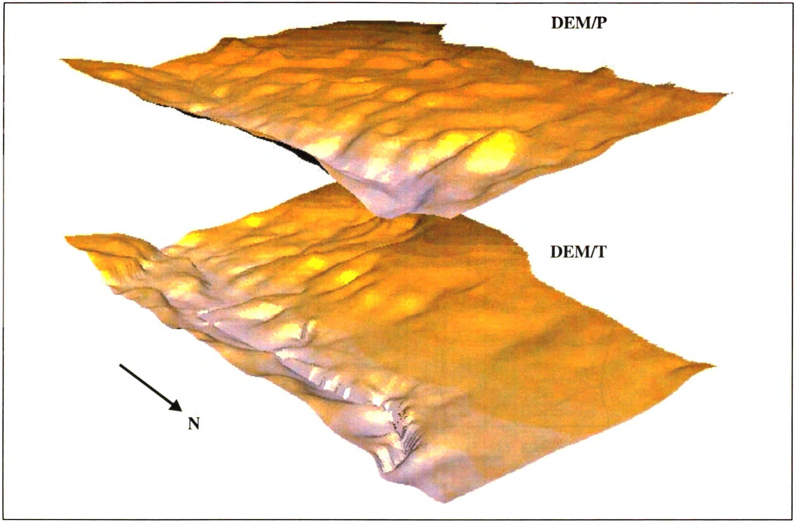

Figure 6. **Shaded relief portrayal of the sampling area (south-west third of Barnard Drain subwatershed) based on DEM/P and DEM/T. Scale varies with perspective, dimensions are 1.8 by 1.2 Km, and vertical exaggeration factor is 12.**

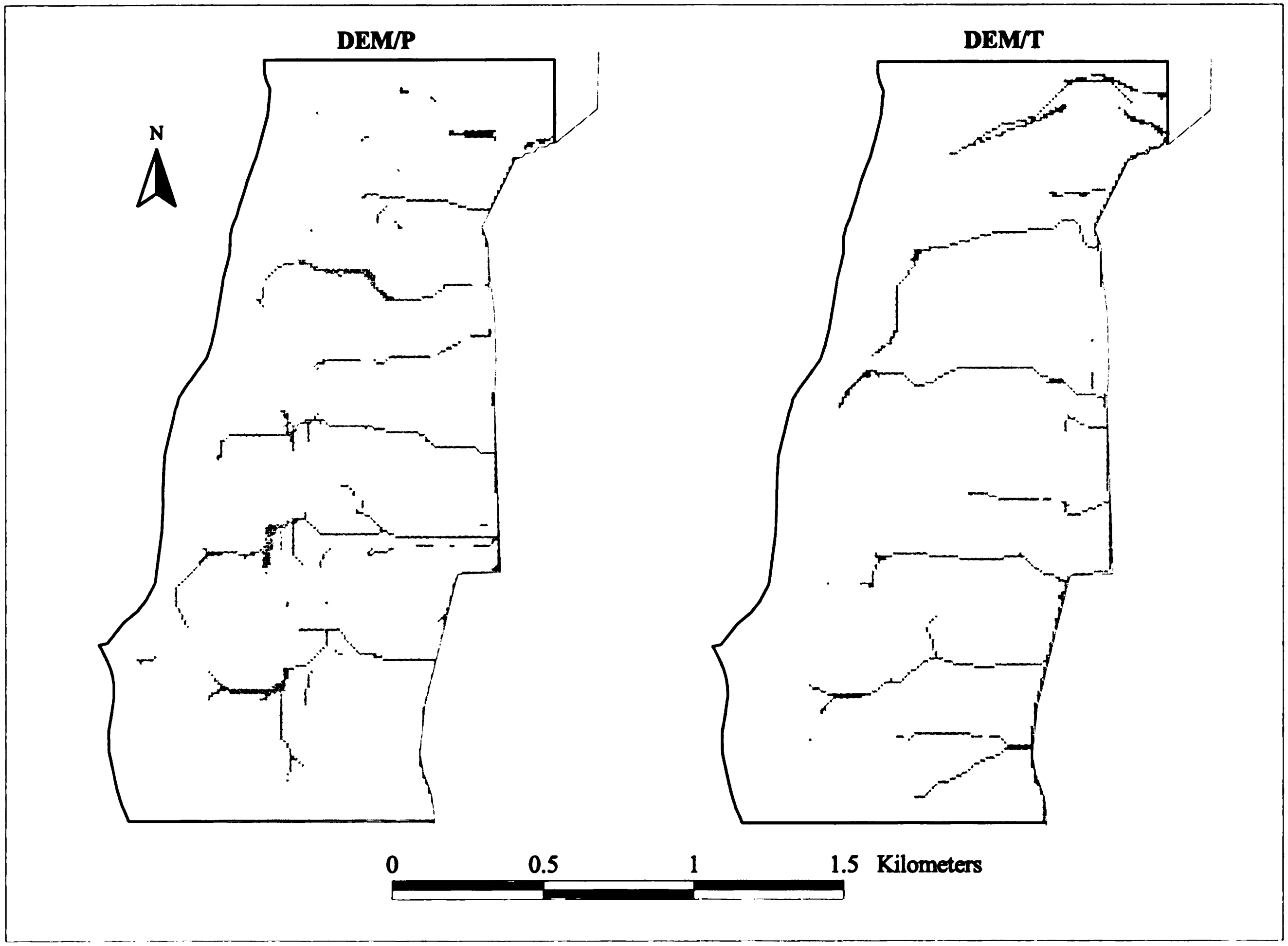

Figure 7. **Cells west of Barnard Drain with $\zeta_{\%} > 95$, as modeled using photogrammetrically (DEM/P) and contour line-interpolated (DEM/T) 10-m digital elevation models, and Barnard Drain center line from USGS DLG file. $\zeta_{\%}$ is an ordinal (percentile) transform of static wetness index calculated using the DEMON flow routing algorithm.**

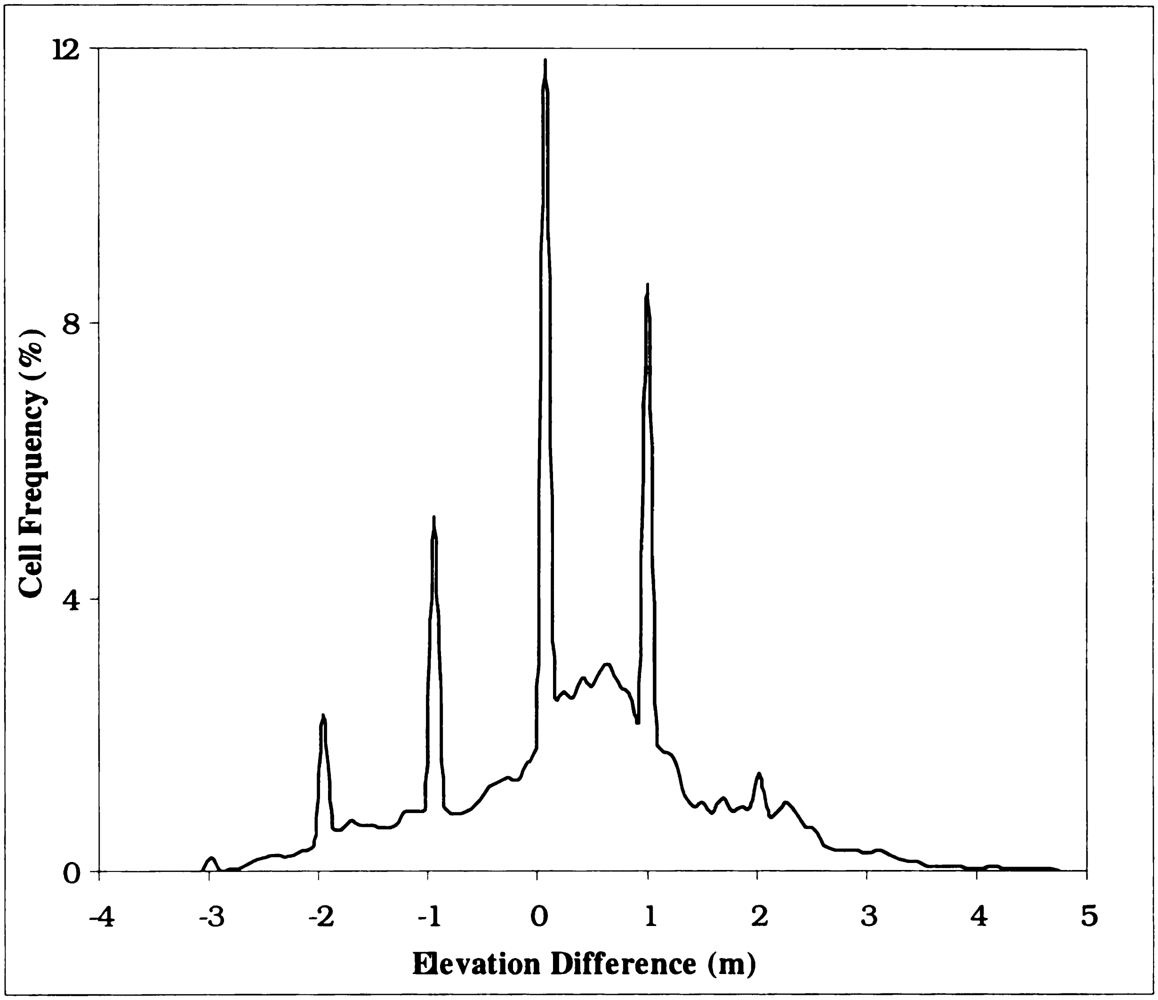

Figure 8. **Frequency distribution for the elevation difference E_P-E_T between elevations derived from photogrammetrically and contour (TOPOGRID) interpolated DEMs on the west side of Barnard Drain.**

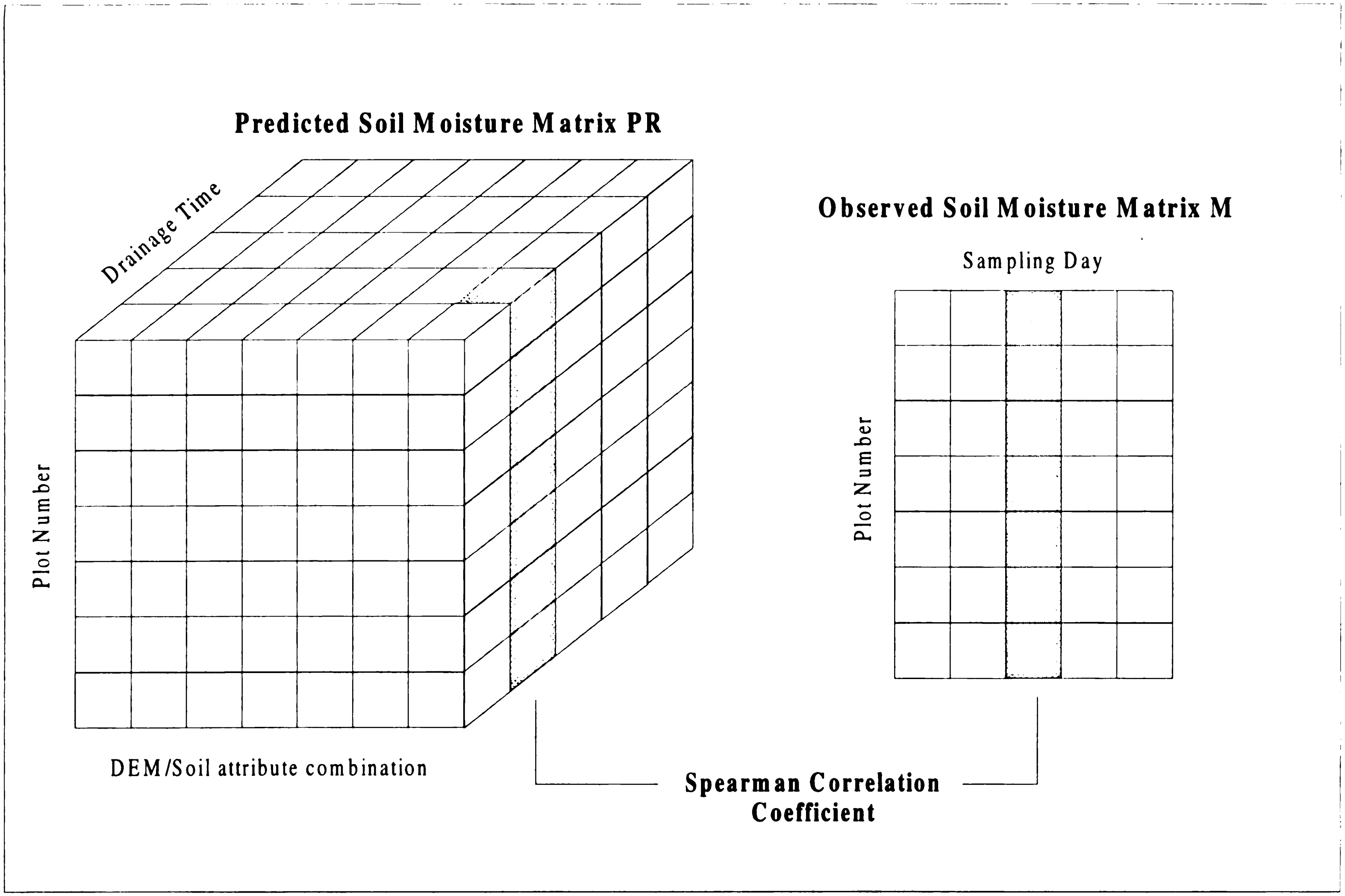

Figure 9. **Conceptual diagram of vector correspondence tested with Spearman's correlation coefficient for Predicted Soil Water Content Matrix PR and Observed Soil Water Content Matrix M.**

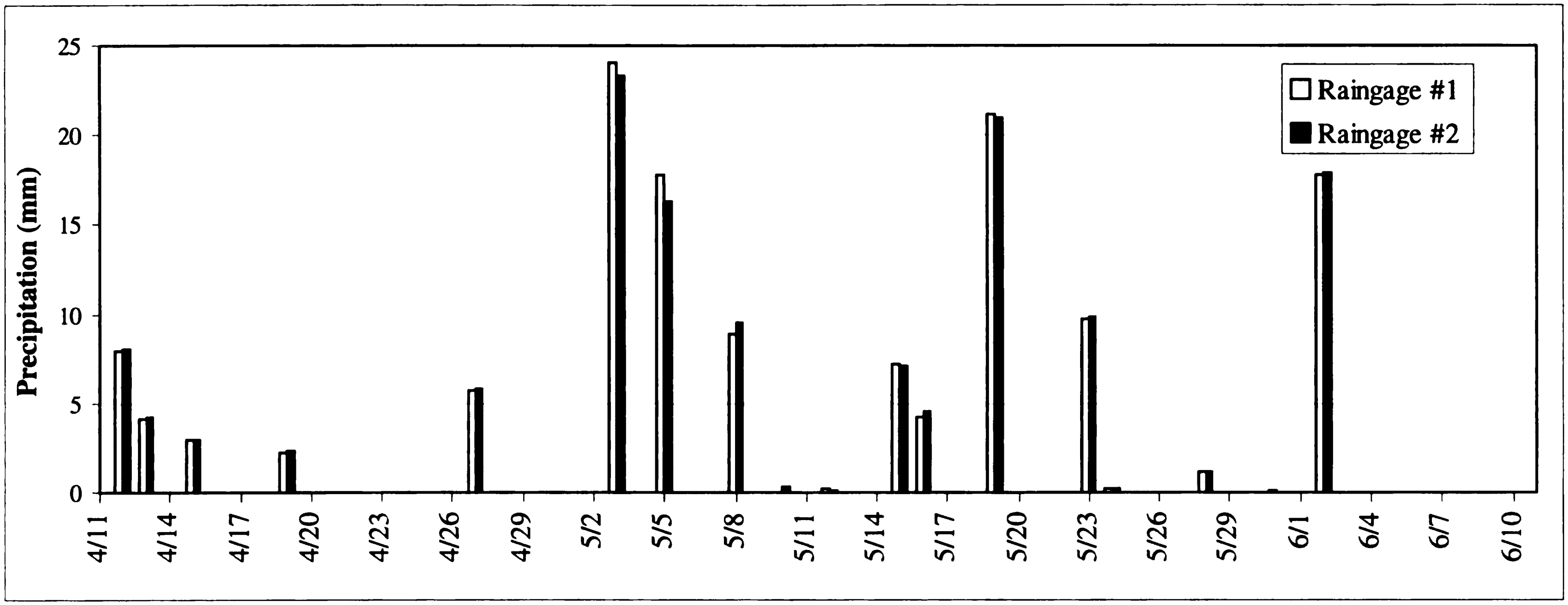

Figure 10. **Rain gage observations for days with precipitation > 0 for the south west third of Barnard Drain watershed.**

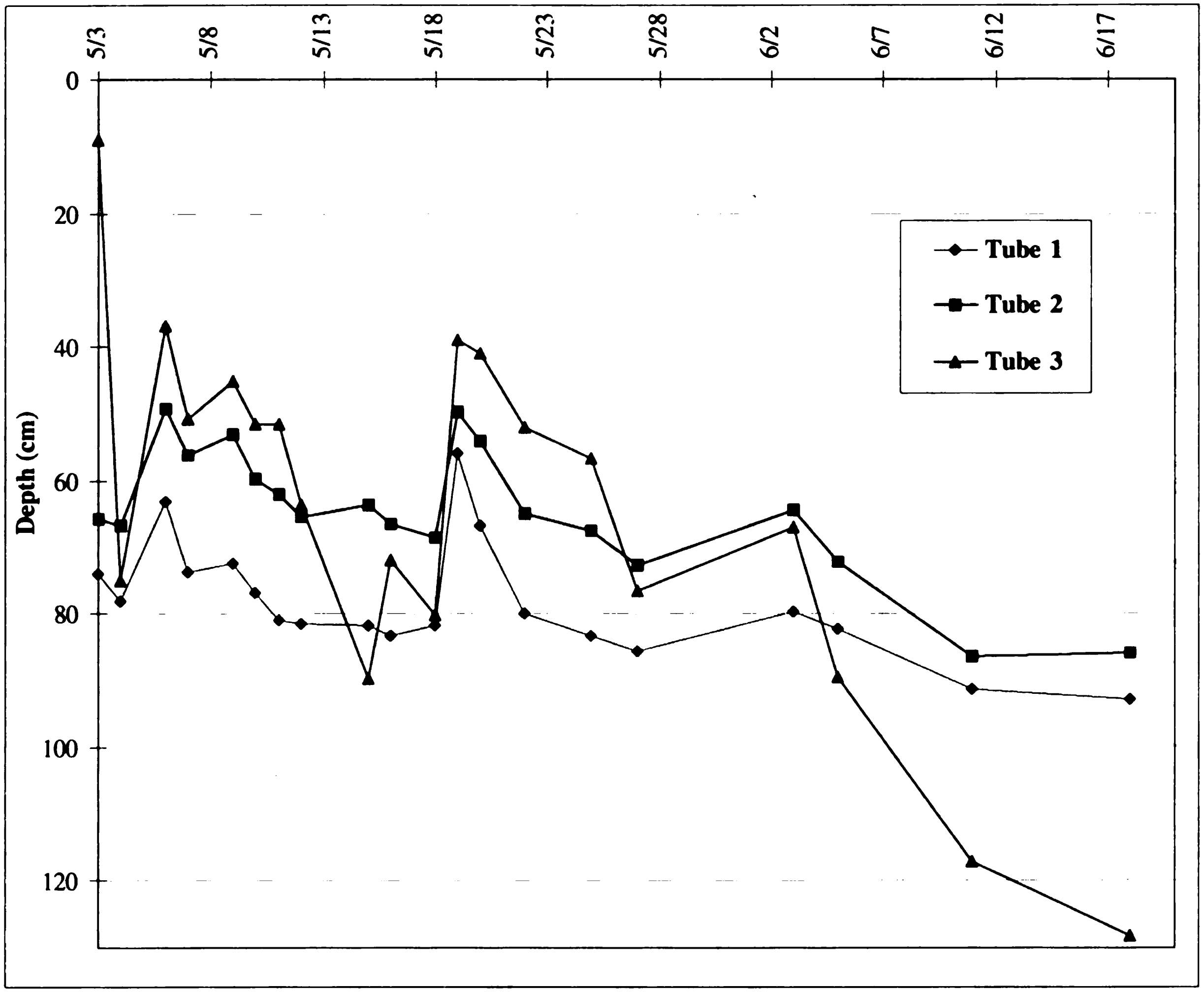

Figure 11. **Water table observations for April 11 to June 10, 1997 in the southwest third of Barnard Drain watershed. High variability of water table depth at location three results from the positioning of the tube exactly on the ephemeral drainage network.**

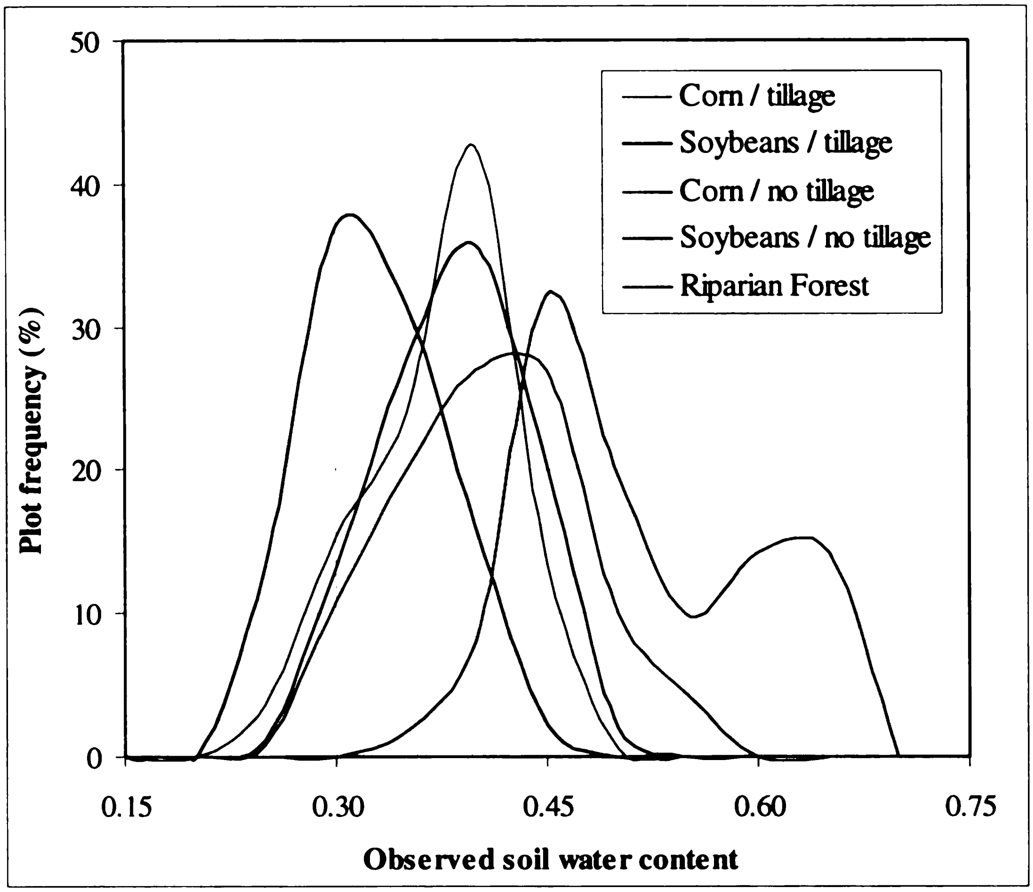

Figure 12. Frequency distribution of observed soil water content (λ) by land use/cover class, pooled across all sampling rounds.

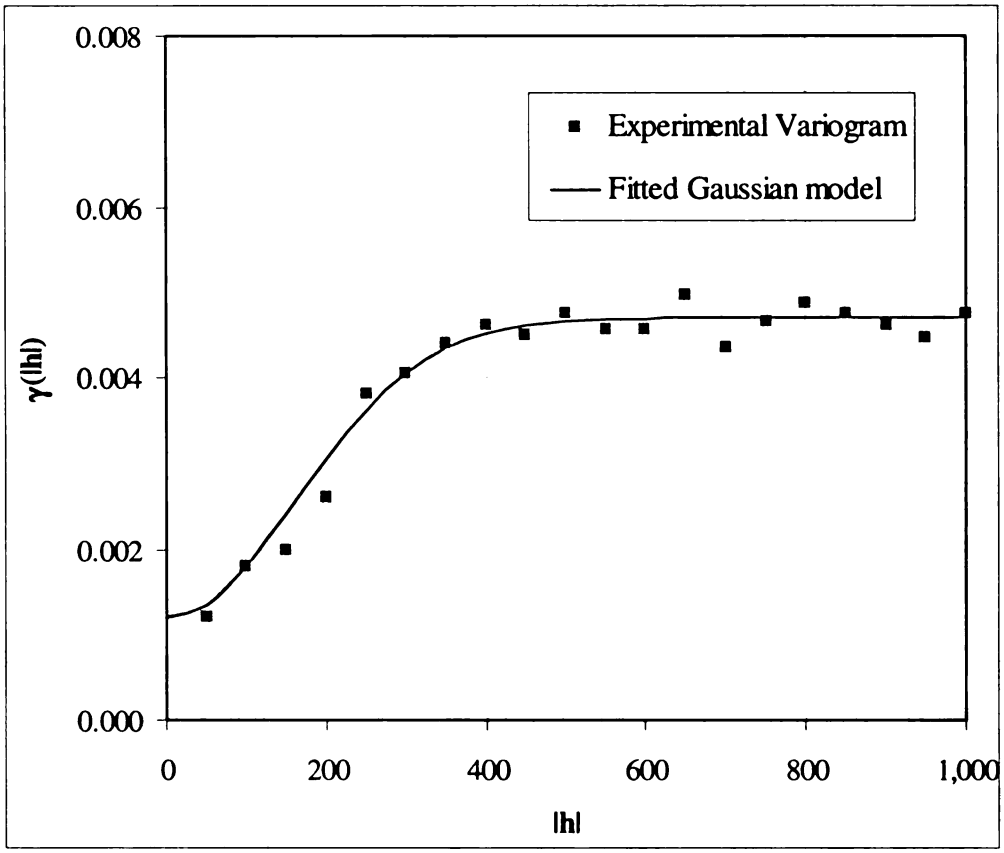

Figure 13. **Omnidirectional variogram of soil water content on April 18, 1997, using Gaussian model form, 50 m lag interval, and 25 m lag tolerance.**

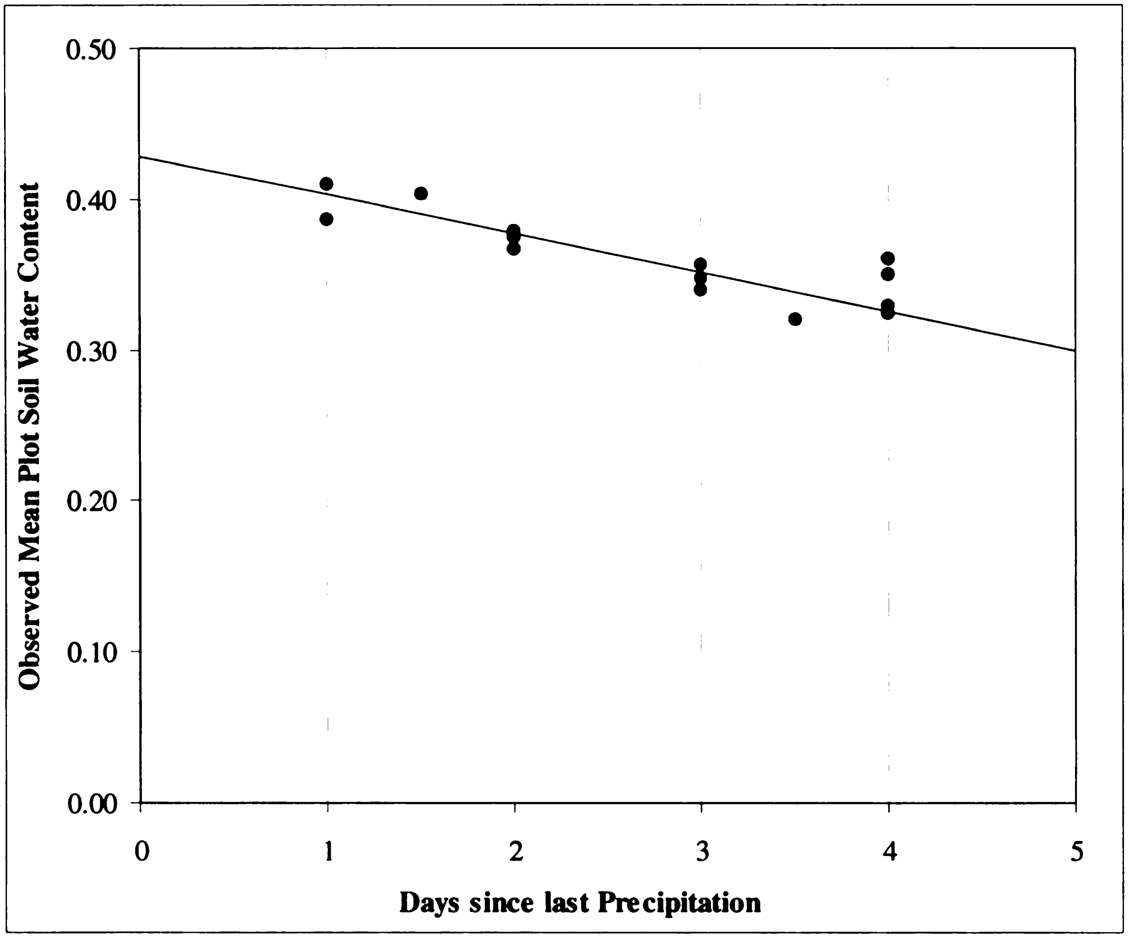

Figure 14. Scatter plot of mean soil water content (for all plots) on time since last precipitation (rounded to the nearest half-day) with fitted regression line (R^2 = 0.864).

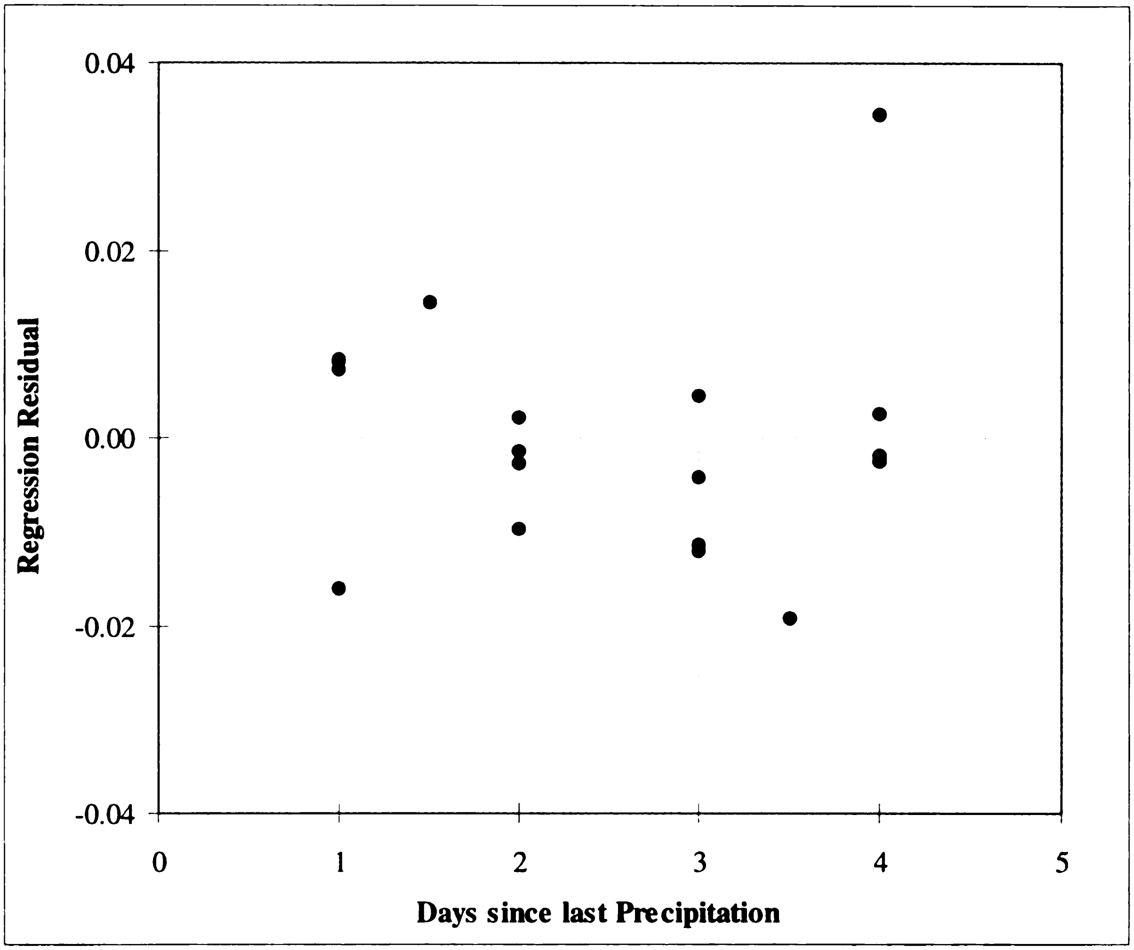

Figure 15. **Plot of the residuals from a regression of mean (all plots) soil water content on time since last precipitation (half days).**

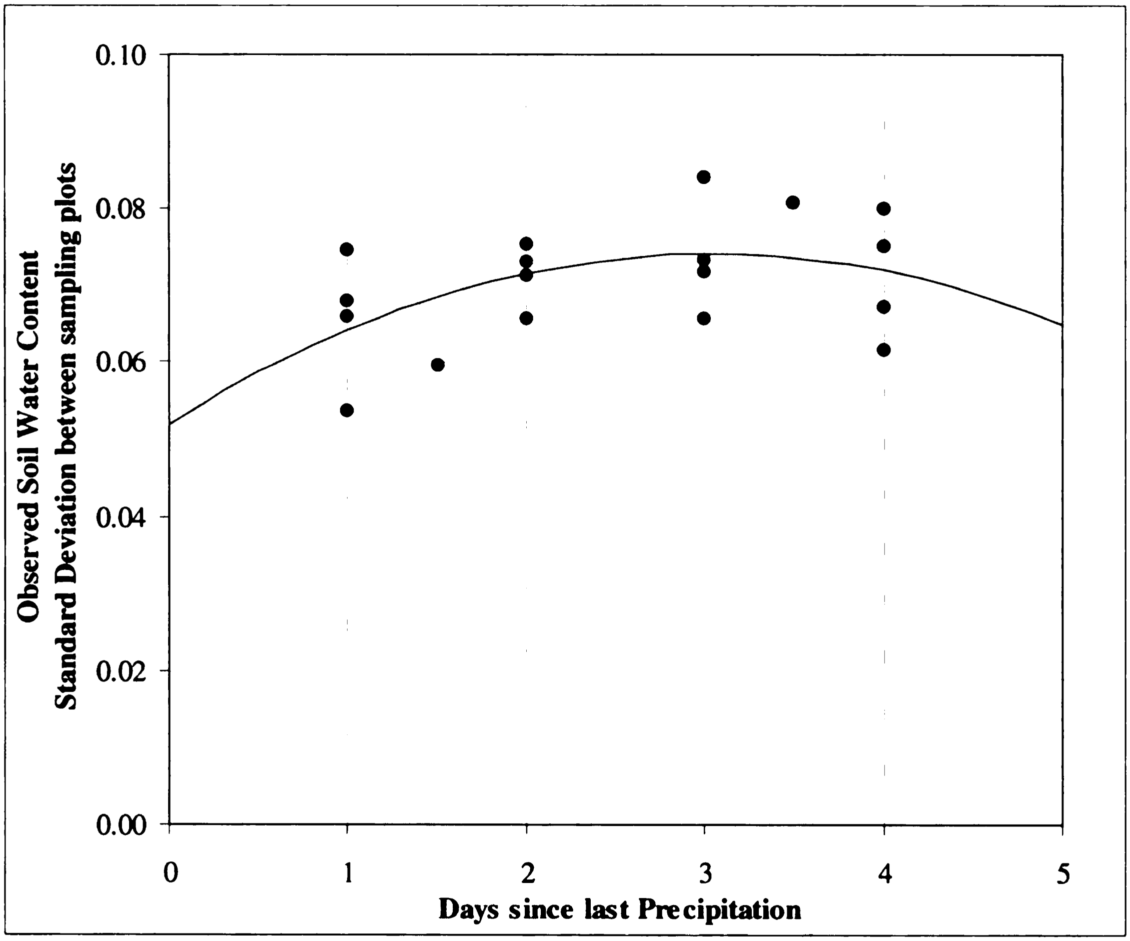

Figure 16. Scatter plot of the per sampling round standard deviation of soil water content (all plots) on time since last precipitation and fitted quadratic regression line ($R^2 = 0.259$).

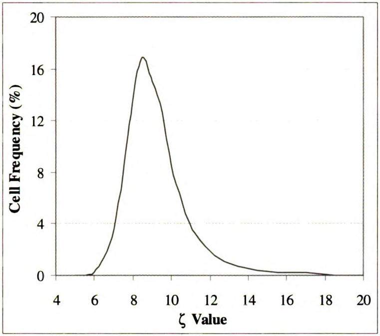

Mean	9.01
Median	8.69
St.Deviation	1.67
Skewness	1.67

Figure 17. Map of Static Wetness Index (ζ) and ζ frequency distribution and summary statistics for cells west of Barnard Drain, as modeled using photogrammetrically generated (DEM/P) 10-m digital elevation model, DEMON flow routing algorithm and slope (derived via the finite difference algorithm).

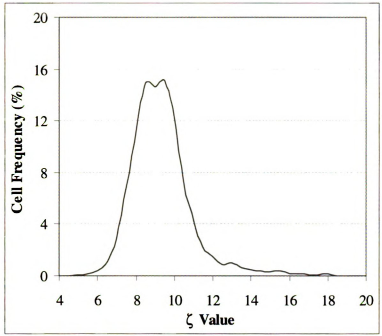

Mean	9.09
Median	8.90
St.Deviation	1.62
Skewness	1.57

Figure 18. Map of Static Wetness Index (ζ) and ζ cell frequency distribution and summary statistics for the area west of Barnard Drain, as modeled using contour line interpolated (DEM/T) 10-m digital elevation model, DEMON flow routing algorithm and slope (derived using the finite difference algorithm).

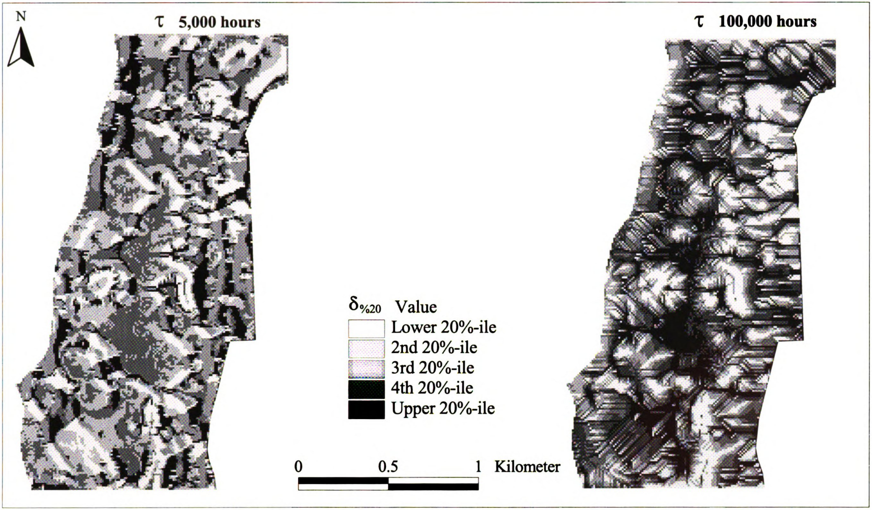

Figure 19. **Modeled $\delta_{\%20}$ classes for cells west of Barnard Drain on a photogrammetrically generated (DEM/P) 10-m digital elevation model. $\delta_{\%20}$ is an ordinal, area defined, 20%-ile transform of dynamic wetness index calculated using uniform soil attributes for two drainage times (τ).**

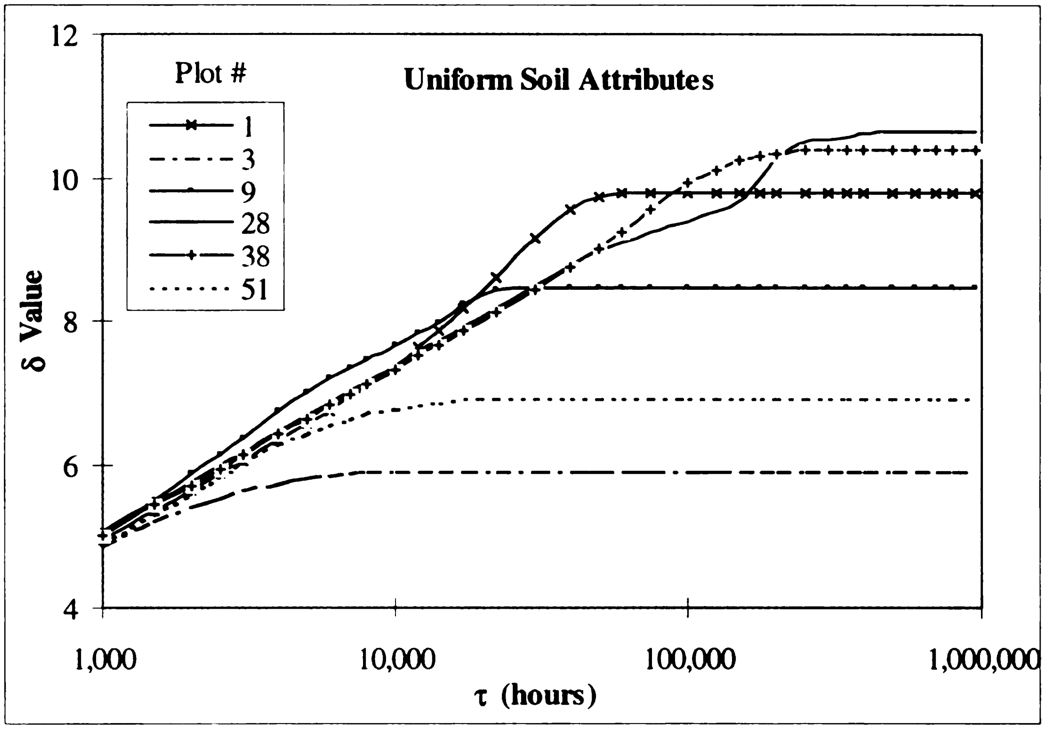

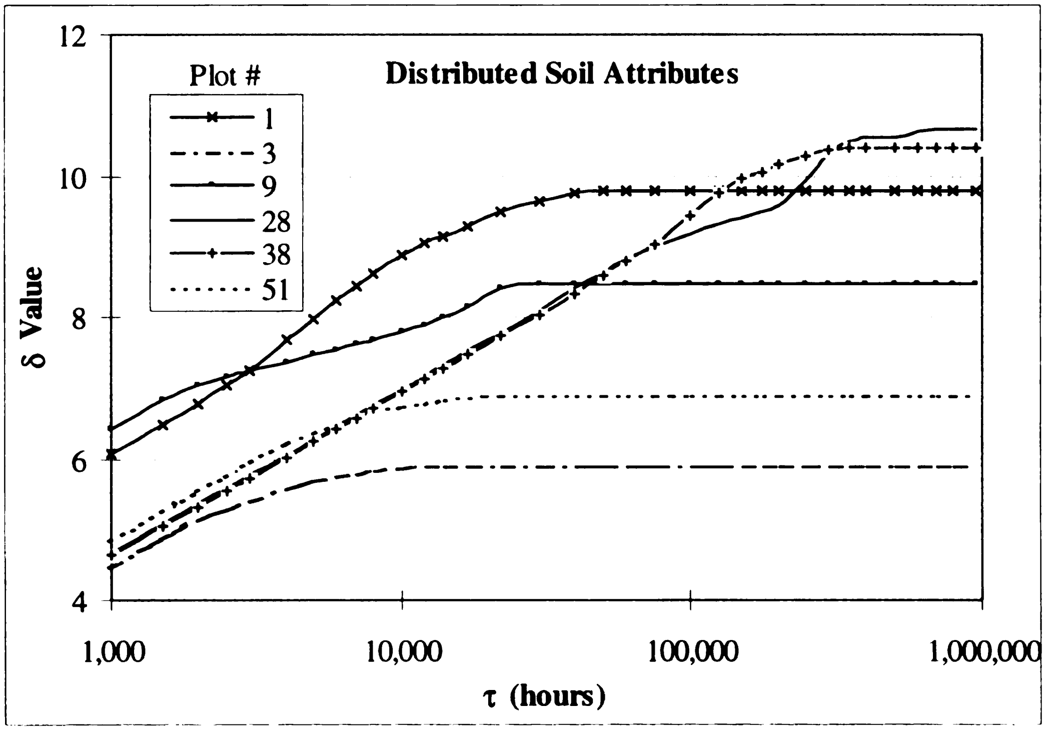

Figure 20. Dynamic wetness index (δ) for a range of Drainage Times (τ) calculated for DEM/P at six sampling plots, and a) Uniform Soil Attributes, and b) Distributed Soil Attributes.

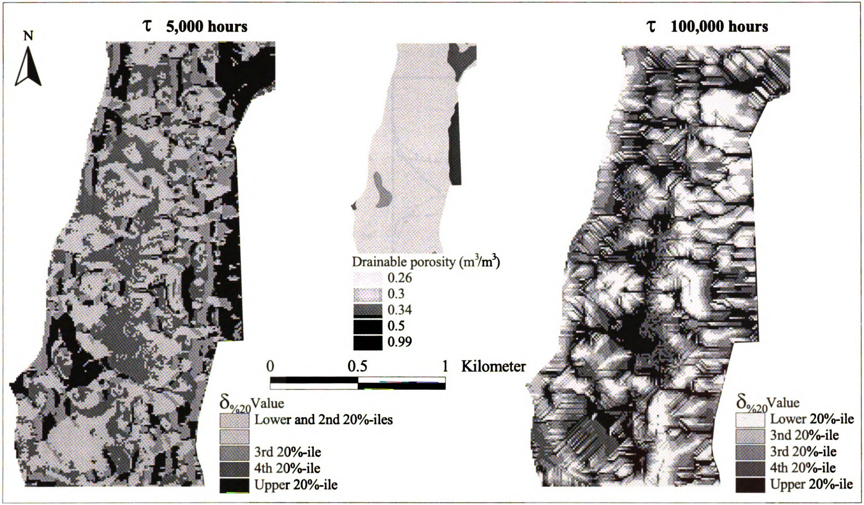

Figure 21. Drainable porosity and modeled $\delta_{\%20}$ classes for cells west of Barnard Drain on a photogrammetrically generated (DEM/P) 10-m digital elevation model for two drainage times (τ). $\delta_{\%20}$ is an ordinal, area defined, 20%-ile transform of dynamic wetness index calculated using distributed soil attributes.

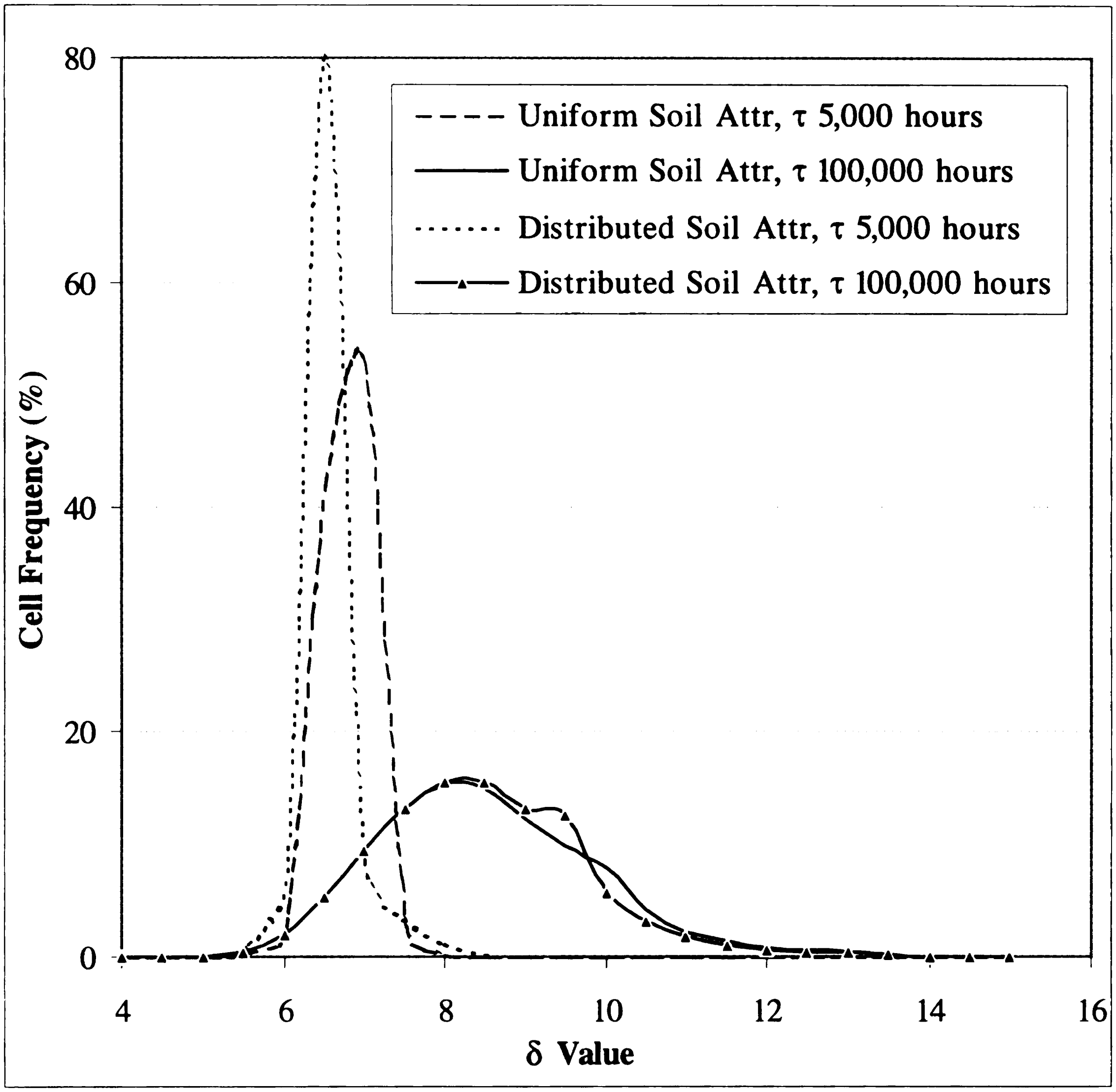

Figure 22. Dynamic wetness index (δ) cell frequency distribution, calculated for DEM/P and four combinations of soil representation and drainage time τ.

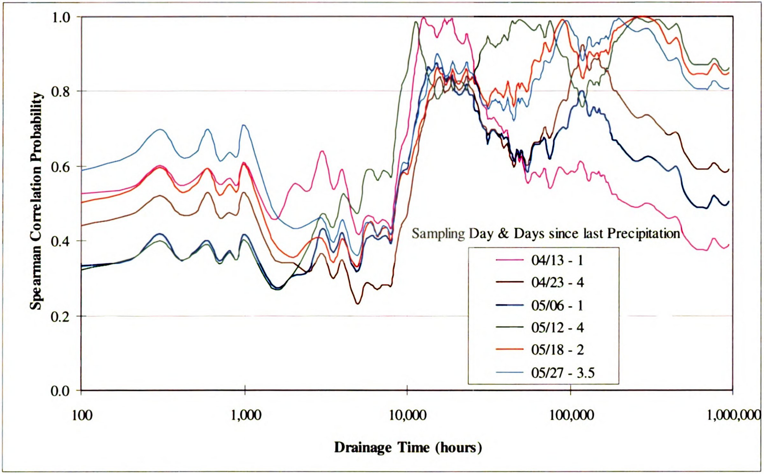

Figure 23. **Spearman rank correlation probability between observed soil water content and corresponding modeled dynamic wetness index (δ) for six sampling days. δ was calculated on DEM/P using uniform soil attributes.**

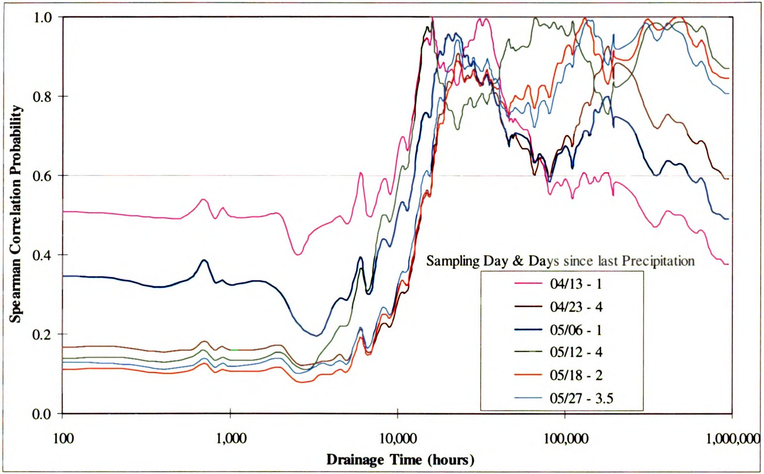

Figure 24. **Spearman rank correlation probability between observed soil water content and corresponding modeled dynamic wetness index (δ) for six sampling days. δ was calculated on DEM/P using distributed soil attributes.**

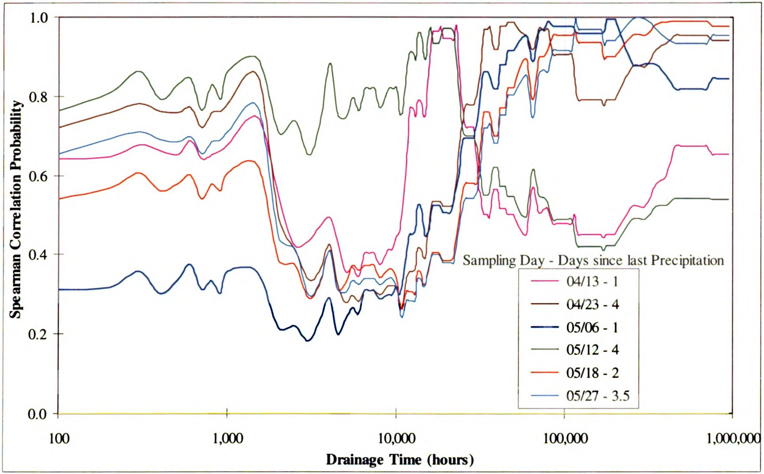

Figure 25. **Spearman rank correlation probability between observed soil water content and corresponding modeled dynamic wetness index (δ) on DEM/P for six sampling days. δ was calculated using a. uniform soil attributes and plots with tillage, b. uniform soil attributes and plots without tillage, c. distributed soil attributes and plots with tillage, and d. distributed soil attributes and plots without tillage.**

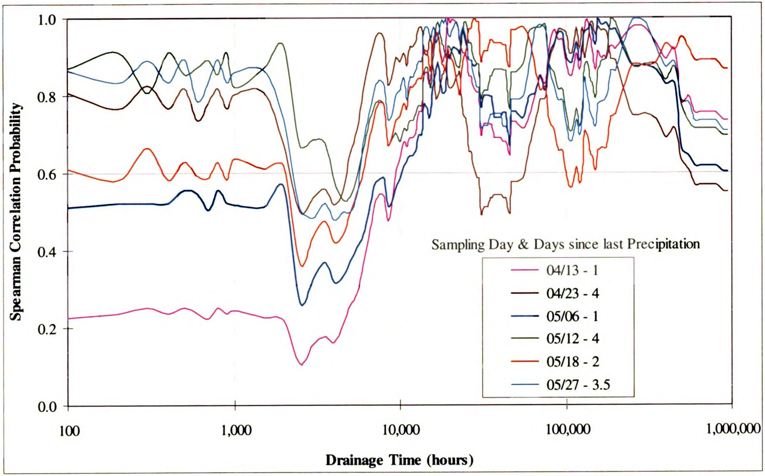
1.0
0.8
0.6
0.4
0.2
0.0
Spearman Correlation Probability
100
1,000
10,000
100,000
1,000,000
Drainage Time (hours)
Sampling Day & Days since last Precipitation
04/13 - 1
04/23 - 4
05/06 - 1
05/12 - 4
05/18 - 2
05/27 - 3.5

Figure 25b.

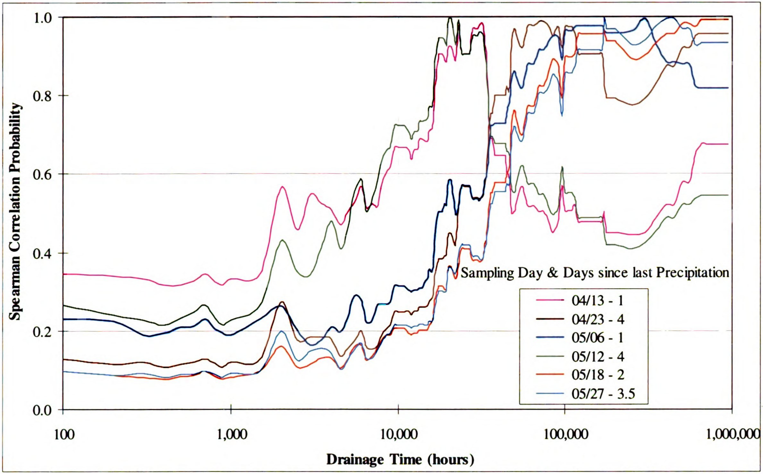
1.0
0.8
0.6
0.4
0.2
0.0
Spearman Correlation Probability
100
1,000
10,000
100,000
1,000,000
Drainage Time (hours)
Sampling Day & Days since last Precipitation
04/13 - 1
04/23 - 4
05/06 - 1
05/12 - 4
05/18 - 2
05/27 - 3.5

Figure 25c.

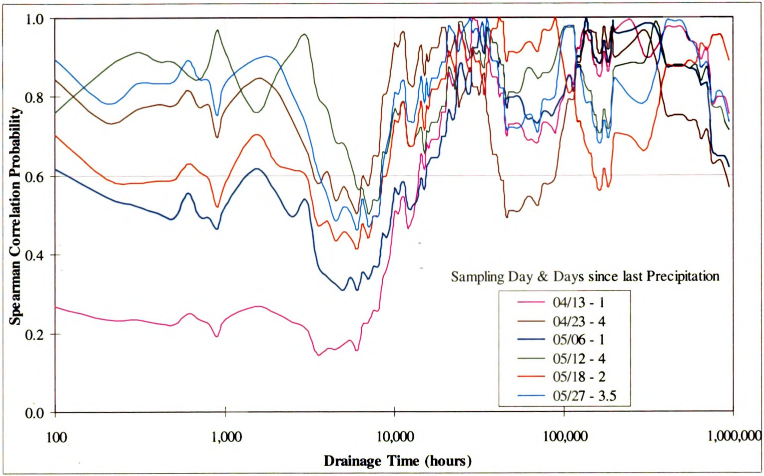
1.0
0.8
0.6
0.4
0.2
0.0
Spearman Correlation Probability
100
1,000
10,000
100,000
1,000,000
Drainage Time (hours)
Sampling Day & Days since last Precipitation
04/13 - 1
04/23 - 4
05/06 - 1
05/12 - 4
05/18 - 2
05/27 - 3.5

Figure 25d.

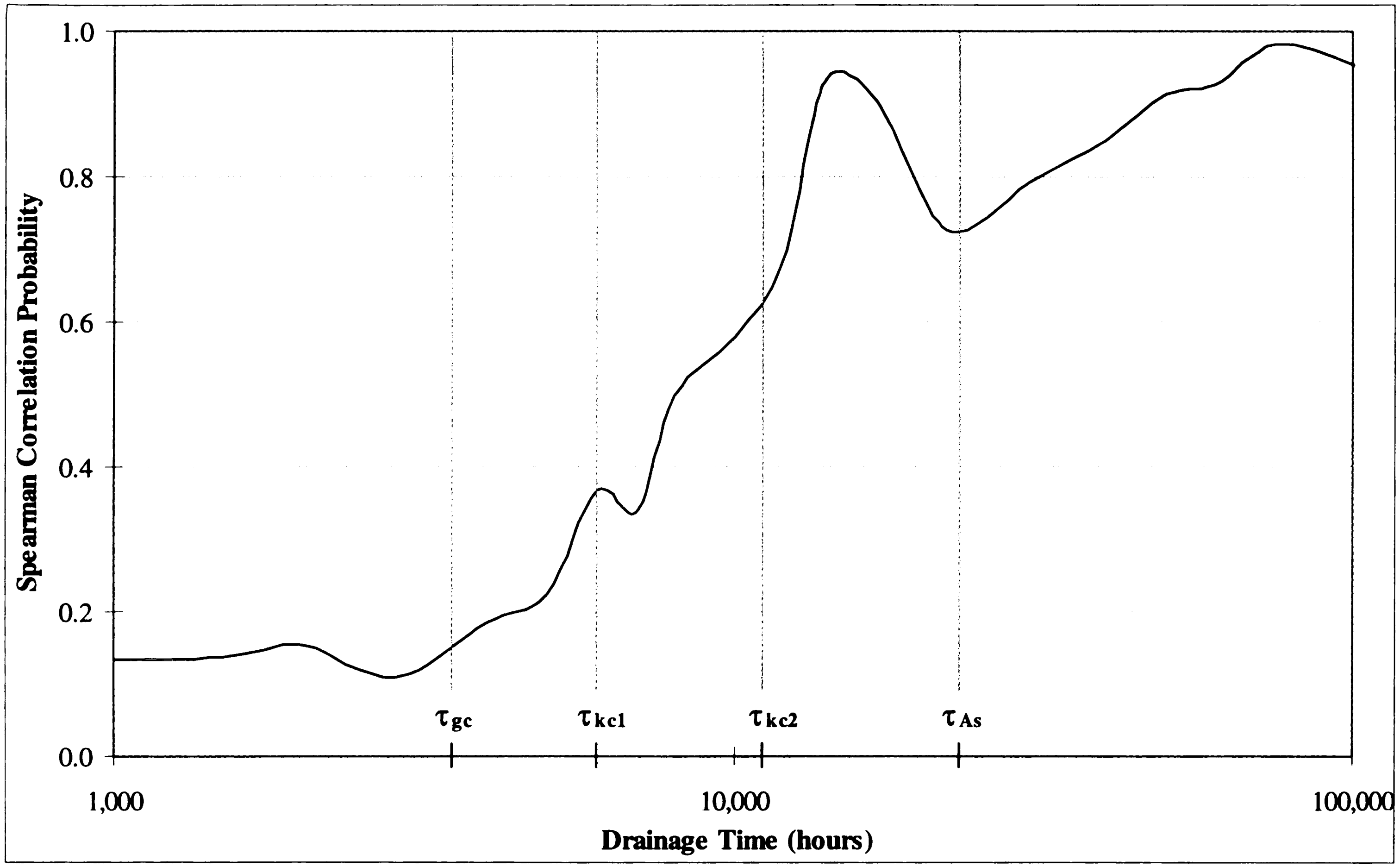

Figure 26. Spearman rank correlation probability between observed soil water content for May 12, 1997 and dynamic wetness index calculated on DEM/P using distributed soil attributes.

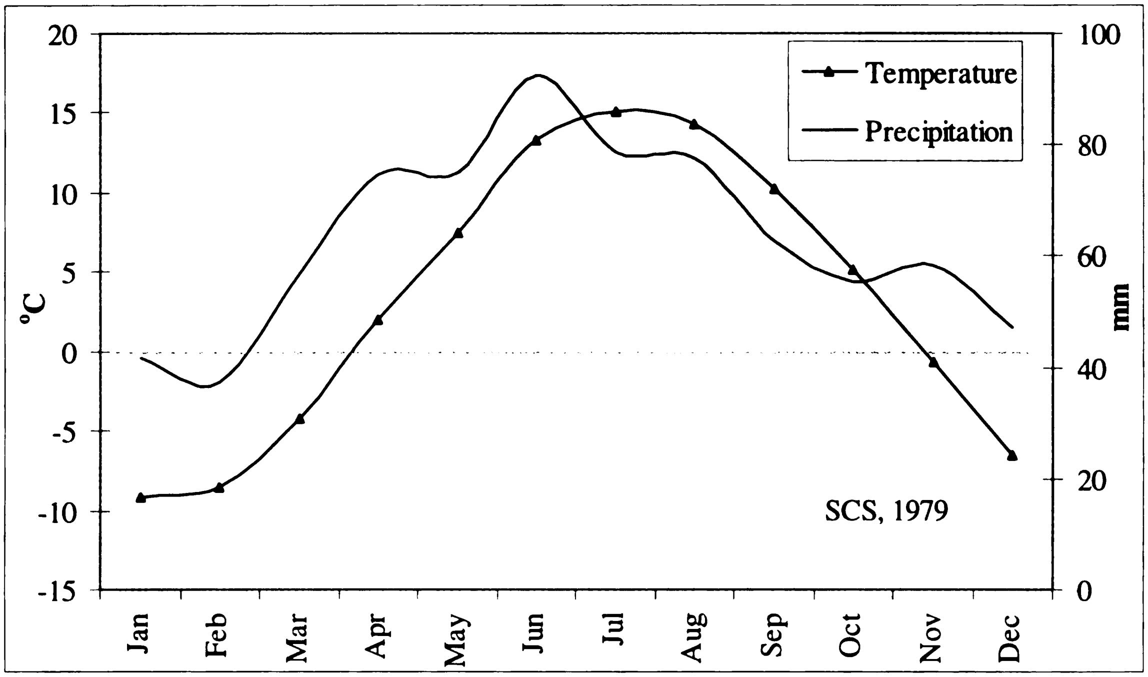

Figure 27. Mean minimum monthly temperature and mean monthly precipitation, calculated from observations at the East Lansing, Michigan, station for the period 1947-1976.

APPENDICES

APPENDIX A

Approaches to improving DEM quality

The quality of DEMs constructed from contour lines depends in part on the relationship between the resolution of the DEM and the contour interval. Where steep slopes are present, the DEM resolution should be equal to the contour interval or finer. Otherwise, two or more contour lines can go through the same grid-cell causing unpredictable errors in cell coding and elevation interpolation (Bitelli et al., 1993). Although the terrain in our sampling area is very gentle, the selected resolution (10 m) is more than three times coarser than the contour interval (10 ft or 3.05m). Thus we investigated the option of building an intermediate TIN structure from the contour lines, to be rasterized afterwards to a DEM with the preferred resolution. The TIN was constructed with the ArcInfo TIN generator, with vectorized versions of the Barnard Drain and GPS recorded drainage paths within the sampling serving as break lines.

The TIN, however, proved unable to correctly handle the terrain morphology of local elevation maxima and of areas in the proximity of Barnard Drain, leading to large flat triangles that would ultimately result in excessive, unrealistic terraced areas in the DEM to be derived. Thus the TIN based DEM was eliminated from further consideration.

APPENDIX B

Calibration of soil water content measurements

Soil water content was measured using a ThetaProbe[8], a soil moisture sensor which enables estimation of volumetric soil water content, ϑ_v, from changes in the apparent soil dielectric constant ε. These changes are converted into DC voltage, which is proportional to soil water content over a wide operating range. Calibration of the relationship between the ThetaProbe voltage output and ϑ_v provides volumetric soil water content measurement accuracy of ±0.01 m^3/m^3.

The soil dielectric constant ε sensed by the probe is related to ϑ by the function:

$$\sqrt{\varepsilon} = a_0 + a_1\vartheta \tag{1}$$

(Whalley, W.R, 1993. White et al., 1994). Because the relationship between $\sqrt{\varepsilon}$ and V (see below) had already been calibrated by the probe vendor, it was only necessary to determine the α_0 and α_1 in order to calculate ϑ_v. Samples of soil for calibration were collected throughout the sampling period spanning a range of drainage stages and soil water content regimes. To minimize potential changes in soil properties such as bulk density, samples were extracted from the ground as cores in metal cylinders. For each sample, voltage output from the probe V_w was recorded, and the sample weight W_w and

[8] Model ML1-UM-2. DELTA-T DEVICES LTD, 128 Low Road, Burwell, Cambridge CB5 0EJ, England

volume L were measured. Samples were oven-dried for 48 hours at 105^0C, re-weighted and re-sampled via ThetaProbe to obtain dry weights W_0 and voltages V_0. The equation:

$$\sqrt{\varepsilon} = 1 + 6.25V - 5.96V^2 + 4.39V^3 \tag{2}$$

found by the probe vendor to fit the (ε, V) relationship precisely ($R^2 = 0.9993$), was then used to calculate $\sqrt{\varepsilon_0}$ and $\sqrt{\varepsilon_w}$. In an oven-dry sample, ϑ_v = 0, and from (1): $\sqrt{\varepsilon_0} = \alpha_0$.

Because

$$\vartheta_v = {(W_w - W_0)}/{L} \tag{3}$$

α_1 can be calculated as

$$\alpha_1 = {(\sqrt{\varepsilon_w} - \sqrt{\varepsilon_0})}/{\vartheta_v} \tag{4}$$

By inverting (1) and substituting (2), the calibrated relationship between ϑ_v and V becomes

$$\vartheta_v = \frac{[1 + 6.25V - 5.96V^2 + 4.39V^3] - \alpha_0}{\alpha_1} \tag{5}$$

This ThetaProbe calibration procedure was applied to 140 soil samples randomly selected from within sample plots in each of the five conditions. The α_0 and α_1 coefficients thus calculated were then averaged to generate a single calibration equation for each condition. Pre and post disturbance probe calibration equations were derived and applied for conditions where tillage occurred during the sampling period. Calibration data and coefficients are summarized in Figures 28a-g and Tables 9-15.

The accuracy of calibrated ThetaProbe output was assessed via comparison with measurements obtained using a Tectronix Time Domain Reflectometry (TDR) unit. The χ^2 test statistic for goodness of fit between the ThetaProbe and TDR estimates for a sample of 102 observations, distributed evenly across conditions, indicated no significant ($p = 0.995$) difference between these methods.

Table 9. **ThetaProbe calibration data and conversion coefficients for the Corn / no tillage condition.**

Sample	Wet Weight W_w (g)	Dry Weight W_o (g)	Water (g)	Sample Volume (ml)	Bulk Density (g/ml)	Probe Output V_w (V)	Probe Output V_o (V)	$\sqrt{\varepsilon_0}$	α_o	ϑ_v	α_1
1	552.0	490.0	62.0	380	1.289	0.371	0.081	2.723	1.469	0.163	7.680
2	565.1	486.7	78.4	380	1.281	0.447	0.087	2.995	1.502	0.206	7.239
3	558.4	482.5	75.9	380	1.270	0.454	0.091	3.020	1.523	0.200	7.496
4	575.7	492.3	83.4	380	1.296	0.477	0.096	3.102	1.549	0.219	7.075
5	574.5	488.9	85.6	380	1.287	0.478	0.098	3.105	1.559	0.225	6.862
6	588.3	500.1	88.2	380	1.316	0.511	0.101	3.223	1.575	0.232	7.101
7	591.5	498.1	93.4	380	1.311	0.526	0.102	3.277	1.580	0.246	6.905
8	600.0	499.4	100.6	380	1.314	0.561	0.103	3.406	1.585	0.265	6.876
9	603.6	499.7	103.9	380	1.315	0.576	0.105	3.462	1.596	0.273	6.824
10	607.0	497.6	109.4	380	1.309	0.598	0.114	3.545	1.642	0.288	6.612
11	617.2	503.1	114.1	380	1.324	0.613	0.112	3.603	1.631	0.300	6.566
12	621.7	504.0	117.7	380	1.326	0.648	0.116	3.742	1.652	0.310	6.748
13	625.5	502.5	123.0	380	1.322	0.668	0.123	3.824	1.687	0.324	6.603
14	630.1	499.2	130.9	380	1.314	0.697	0.119	3.947	1.667	0.344	6.620
15	638.6	504.1	134.5	380	1.327	0.716	0.124	4.031	1.692	0.354	6.609
16	641.2	497.6	143.6	380	1.309	0.752	0.133	4.196	1.736	0.378	6.511
17	648.5	500.8	147.7	380	1.318	0.760	0.135	4.235	1.746	0.389	6.403
18	648.5	494.4	154.1	380	1.301	0.783	0.138	4.347	1.761	0.406	6.378
19	658.0	496.4	161.6	380	1.306	0.815	0.142	4.511	1.780	0.425	6.423
20	658.6	487.9	170.7	380	1.284	0.840	0.154	4.647	1.837	0.449	6.254
21	669.7	495.5	174.2	380	1.304	0.845	0.143	4.674	1.785	0.458	6.304
22	677.0	494.9	182.1	380	1.302	0.878	0.144	4.864	1.790	0.479	6.416
23	678.4	487.1	191.3	380	1.282	0.899	0.146	4.992	1.799	0.503	6.341
24	685.9	487.4	198.5	380	1.283	0.923	0.152	5.143	1.828	0.522	6.347
25	687.7	483.5	204.2	380	1.272	0.932	0.152	5.202	1.828	0.537	6.279
26	694.5	477.9	216.6	380	1.258	0.978	0.157	5.518	1.851	0.570	6.434
$\bar{x}$					**1.300**				**1.679**		**6.689**
s					**0.020**				**0.115**		**0.379**

Table 10. **ThetaProbe calibration data and conversion coefficients for the Soybeans / no tillage condition.**

Sample	Wet Weight W_w (g)	Dry Weight W_o (g)	Water (g)	Sample Volume (ml)	Bulk Density (g/ml)	Probe Output V_w (V)	Probe Output V_o (V)	$\sqrt{\varepsilon_0}$	α_0	ϑ_v	α_1
1	503.9	450.6	53.3	380	1.186	0.332	0.077	2.579	1.448	0.140	8.062
2	521.1	460.8	60.3	380	1.213	0.375	0.083	2.737	1.480	0.159	7.921
3	546.8	476.6	70.2	380	1.254	0.431	0.095	2.938	1.544	0.185	7.548
4	555.9	467.4	88.5	380	1.230	0.536	0.100	3.314	1.570	0.233	7.488
5	563.5	486.6	76.9	380	1.281	0.467	0.093	3.066	1.533	0.202	7.574
6	581.7	484.4	97.3	380	1.275	0.597	0.101	3.541	1.575	0.256	7.679
7	589.0	491.3	97.7	380	1.293	0.574	0.103	3.454	1.585	0.257	7.268
8	598.8	505.1	93.7	380	1.329	0.579	0.107	3.473	1.606	0.247	7.571
9	606.8	504.4	102.4	380	1.327	0.596	0.108	3.537	1.611	0.269	7.148
10	624.4	502.3	122.1	380	1.322	0.684	0.108	3.891	1.611	0.321	7.097
11	632.5	518.9	113.6	380	1.366	0.665	0.111	3.812	1.626	0.299	7.310
12	641.0	515.6	125.4	380	1.357	0.737	0.112	4.126	1.631	0.330	7.560
13	649.6	525.6	124.0	380	1.383	0.703	0.119	3.973	1.667	0.326	7.069
14	658.1	523.5	134.6	380	1.378	0.784	0.114	4.352	1.642	0.354	7.653
15	673.7	523.6	150.1	380	1.378	0.795	0.126	4.408	1.702	0.395	6.851
16	682.6	521.0	161.6	380	1.371	0.859	0.126	4.754	1.702	0.425	7.176
17	692.3	527.8	164.5	380	1.389	0.870	0.130	4.817	1.721	0.433	7.151
18	700.3	525.2	175.1	380	1.382	0.919	0.131	5.117	1.726	0.461	7.359
19	707.9	532.2	175.7	380	1.401	0.891	0.127	4.942	1.707	0.462	6.998
20	717.8	538.2	179.6	380	1.416	0.905	0.137	5.029	1.756	0.473	6.925
21	734.8	531.8	203.0	380	1.399	0.972	0.136	5.476	1.751	0.534	6.972
$\bar{x}$					**1.330**				**1.628**		**7.352**
s					**0.068**				**0.086**		**0.331**

Table 11. **ThetaProbe calibration data and conversion coefficients for the Soybeans / pre-tillage condition.**

Sample	Wet Weight W_w (g)	Dry Weight W_o (g)	Water (g)	Sample Volume (ml)	Bulk Density (g/ml)	Probe Output V_w (V)	Probe Output V_o (V)	$\sqrt{\varepsilon_0}$	α_o	ϑ_v	α_1
1	487.2	431.3	55.9	380	1.135	0.365	0.050	2.701	1.298	0.147	9.534
2	494.6	433.2	61.4	380	1.140	0.396	0.053	2.813	1.317	0.162	9.261
3	511.0	444.3	66.7	380	1.169	0.394	0.062	2.806	1.366	0.176	8.205
4	510.9	448.2	62.7	380	1.179	0.415	0.047	2.881	1.281	0.165	9.697
5	532.7	451.0	81.7	380	1.187	0.513	0.066	3.230	1.386	0.215	8.577
6	547.0	449.4	97.6	380	1.183	0.610	0.066	3.591	1.387	0.257	8.581
7	554.5	468.4	86.1	380	1.233	0.538	0.072	3.321	1.423	0.227	8.378
8	562.9	464.9	98.0	380	1.223	0.615	0.074	3.611	1.430	0.258	8.455
9	585.0	478.1	106.9	380	1.258	0.658	0.081	3.783	1.468	0.281	8.227
10	593.1	478.3	114.8	380	1.259	0.678	0.077	3.866	1.450	0.302	7.997
11	600.1	485.5	114.6	380	1.278	0.700	0.081	3.960	1.472	0.302	8.252
12	608.4	473.1	135.3	380	1.245	0.792	0.107	4.392	1.606	0.356	7.826
13	629.8	492.5	137.3	380	1.296	0.795	0.090	4.408	1.518	0.361	7.999
14	636.6	493.8	142.8	380	1.299	0.821	0.098	4.543	1.557	0.376	7.946
15	645.1	488.4	156.7	380	1.285	0.874	0.096	4.841	1.550	0.412	7.980
16	652.8	490.4	162.4	380	1.291	0.888	0.100	4.924	1.568	0.427	7.854
17	668.0	490.3	177.7	380	1.290	0.942	0.105	5.268	1.595	0.468	7.856
18	674.1	496.8	177.3	380	1.307	0.956	0.108	5.364	1.608	0.467	8.048
19	683.1	482.1	201.0	380	1.269	1.009	0.138	5.748	1.761	0.529	7.539
20	690.8	481.7	209.1	380	1.268	1.023	0.144	5.856	1.790	0.550	7.391
$\bar{x}$					**1.240**				**1.491**		**8.280**
s					**0.056**				**0.140**		**0.611**

Table 12. ThetaProbe calibration data and conversion coefficients for the Soybeans / post-tillage condition.

Sample	Wet Weight W_w (g)	Dry Weight W_o (g)	Water (g)	Sample Volume (ml)	Bulk Density (g/ml)	Probe Output V_w (V)	Probe Output V_o (V)	$\sqrt{\varepsilon_0}$	α_o	ϑ_v	α_1
1	487.5	435.2	52.3	380	1.145	0.319	0.064	2.530	1.377	0.138	8.378
2	494.3	443.7	50.6	380	1.168	0.339	0.058	2.605	1.343	0.133	9.474
3	506.2	433.1	73.1	380	1.140	0.438	0.059	2.963	1.349	0.192	8.391
4	520.7	448.2	72.5	380	1.179	0.461	0.069	3.045	1.404	0.191	8.598
5	528.2	429.5	98.7	380	1.130	0.579	0.079	3.473	1.459	0.260	7.754
6	533.7	449.8	83.9	380	1.184	0.491	0.066	3.152	1.388	0.221	7.988
7	541.3	445.2	96.1	380	1.172	0.568	0.075	3.432	1.437	0.253	7.887
8	548.7	457.6	91.1	380	1.204	0.531	0.078	3.296	1.453	0.240	7.684
9	555.4	460.6	94.8	380	1.212	0.595	0.076	3.533	1.443	0.249	8.382
10	567.9	457.0	110.9	380	1.203	0.657	0.078	3.779	1.453	0.292	7.968
11	567.3	462.9	104.4	380	1.218	0.635	0.085	3.690	1.491	0.275	8.003
12	589.3	466.3	123.0	380	1.227	0.698	0.086	3.952	1.496	0.324	7.586
13	595.3	467.4	127.9	380	1.230	0.723	0.088	4.062	1.507	0.337	7.593
14	602.8	468.1	134.7	380	1.232	0.756	0.091	4.215	1.523	0.354	7.597
15	609.1	468.3	140.8	380	1.232	0.796	0.088	4.413	1.507	0.371	7.843
16	615.2	490.2	125.0	380	1.290	0.744	0.097	4.159	1.554	0.329	7.918
17	637.3	473.2	164.1	380	1.245	0.879	0.096	4.870	1.549	0.432	7.691
18	643.8	471.4	172.4	380	1.241	0.914	0.098	5.086	1.559	0.454	7.772
19	650.3	470.2	180.1	380	1.237	0.935	0.106	5.222	1.601	0.474	7.640
20	656.5	454.2	202.3	380	1.195	0.996	0.117	5.650	1.657	0.532	7.501
21	664.0	453.0	211.0	380	1.192	1.023	0.135	5.856	1.746	0.555	7.403
22	691.0	491.2	199.8	380	1.293	1.002	0.143	5.695	1.785	0.526	7.437
$\bar{x}$					**1.208**				**1.504**		**7.931**
s					**0.043**				**0.116**		**0.477**

Table 13. ThetaProbe calibration data and conversion coefficients for the Corn / pre-tillage condition.

Sample	Wet Weight W_w (g)	Dry Weight W_o (g)	Water (g)	Sample Volume (ml)	Bulk Density (g/ml)	Probe Output V_w (V)	Probe Output V_o (V)	$\sqrt{\varepsilon_0}$	α_o	ϑ_v	α_1
1	480.1	419.4	60.7	380	1.104	0.356	0.059	2.668	1.351	0.160	8.242
2	495.8	439.2	56.6	380	1.156	0.328	0.057	2.565	1.340	0.149	8.230
3	480.0	420.0	60.0	380	1.105	0.368	0.078	2.712	1.453	0.158	7.971
4	499.2	431.2	68.0	380	1.135	0.436	0.068	2.957	1.399	0.179	8.707
5	542.7	445.1	97.6	380	1.171	0.563	0.083	3.414	1.479	0.257	7.531
6	544.4	443.6	100.8	380	1.167	0.612	0.093	3.599	1.534	0.265	7.784
7	550.2	462.1	88.1	380	1.216	0.560	0.095	3.403	1.546	0.232	8.011
8	571.5	448.7	122.8	380	1.181	0.693	0.098	3.930	1.558	0.323	7.342
9	597.8	467.4	130.4	380	1.230	0.721	0.112	4.053	1.629	0.343	7.065
10	604.2	452.7	151.5	380	1.191	0.803	0.113	4.451	1.636	0.399	7.062
11	609.5	473.6	135.9	380	1.246	0.781	0.118	4.337	1.660	0.358	7.486
12	630.3	468.7	161.6	380	1.233	0.847	0.131	4.687	1.724	0.425	6.967
13	645.4	469.5	175.9	380	1.236	0.906	0.138	5.035	1.761	0.463	7.073
14	652.1	470.4	181.7	380	1.238	0.938	0.156	5.242	1.847	0.478	7.100
15	657.5	444.7	212.8	380	1.170	1.005	0.146	5.718	1.801	0.560	6.994
16	665.9	467.2	198.7	380	1.229	0.991	0.175	5.613	1.935	0.523	7.035
$\bar{x}$					**1.188**				**1.603**		**7.537**
s					**0.047**				**0.178**		**0.553**

Table 14. **ThetaProbe calibration data and conversion coefficients for the Corn / post-tillage condition.**

Sample	Wet Weight W_w (g)	Dry Weight W_o (g)	Water (g)	Sample Volume (ml)	Bulk Density (g/ml)	Probe Output V_w (V)	Probe Output V_o (V)	$\sqrt{\varepsilon_0}$	α_o	ϑ_v	α_1
1	457.6	406.1	51.5	380	1.069	0.337	0.058	2.597	1.343	0.136	9.253
2	502.3	445.0	57.3	380	1.171	0.379	0.061	2.752	1.360	0.151	9.229
3	466.3	393.3	73.0	380	1.035	0.465	0.064	3.059	1.377	0.192	8.757
4	483.2	416.6	66.6	380	1.096	0.405	0.067	2.845	1.393	0.175	8.285
5	461.3	399.0	62.3	380	1.050	0.445	0.075	2.988	1.437	0.164	9.459
6	499.2	430.2	69.0	380	1.132	0.452	0.076	3.013	1.443	0.182	8.648
7	493.2	410.4	82.8	380	1.080	0.536	0.097	3.314	1.554	0.218	8.075
8	501.2	434.6	66.6	380	1.144	0.456	0.101	3.027	1.575	0.175	8.285
9	522.4	432.3	90.1	380	1.138	0.553	0.103	3.376	1.585	0.237	7.552
10	529.9	434.8	95.1	380	1.144	0.583	0.109	3.488	1.616	0.250	7.479
11	535.6	431.7	103.9	380	1.136	0.623	0.099	3.642	1.565	0.273	7.598
12	557.6	451.6	106.0	380	1.188	0.647	0.116	3.738	1.652	0.279	7.479
13	571.8	459.6	112.2	380	1.209	0.669	0.134	3.828	1.741	0.295	7.069
14	588.0	459.7	128.3	380	1.210	0.748	0.122	4.178	1.682	0.338	7.392
15	592.8	457.2	135.6	380	1.203	0.749	0.127	4.182	1.707	0.357	6.938
16	604.4	469.1	135.3	380	1.234	0.782	0.128	4.342	1.712	0.356	7.388
17	612.3	463.8	148.5	380	1.221	0.813	0.135	4.501	1.746	0.391	7.050
18	618.3	455.8	162.5	380	1.199	0.867	0.135	4.800	1.746	0.428	7.141
19	639.9	461.5	178.4	380	1.214	0.956	0.144	5.364	1.790	0.469	7.613
20	646.2	460.5	185.7	380	1.212	0.967	0.149	5.440	1.813	0.489	7.421
21	659.8	446.3	213.5	380	1.174	1.003	0.175	5.703	1.935	0.562	6.706
$\bar{x}$					**1.155**				**1.608**		**7.848**
s					**0.060**				**0.167**		**0.816**

Table 15. ThetaProbe calibration data and conversion coefficients for the Forested condition.

Sample	Wet Weight W_w (g)	Dry Weight W_o (g)	Water (g)	Sample Volume (ml)	Bulk Density (g/ml)	Probe Output V_w (V)	Probe Output V_o (V)	$\sqrt{\varepsilon_0}$	α_o	ϑ_v	α_1
1	648.5	536.8	111.7	380	1.413	0.648	0.092	3.742	1.528	0.294	7.532
2	650.3	533.9	116.4	380	1.405	0.672	0.096	3.841	1.549	0.306	7.482
3	657.0	535.7	121.3	380	1.410	0.691	0.101	3.921	1.575	0.319	7.351
4	656.6	530.3	126.3	380	1.396	0.710	0.109	4.004	1.616	0.332	7.185
5	663.6	532.0	131.6	380	1.400	0.738	0.111	4.131	1.626	0.346	7.232
6	667.8	530.6	137.2	380	1.396	0.766	0.111	4.264	1.626	0.361	7.304
7	677.3	534.5	142.8	380	1.407	0.788	0.118	4.372	1.662	0.376	7.213
8	681.2	532.3	148.9	380	1.401	0.804	0.113	4.454	1.636	0.392	7.190
9	686.6	531.6	155.0	380	1.399	0.839	0.119	4.641	1.667	0.408	7.292
10	694.1	532.5	161.6	380	1.401	0.828	0.123	4.581	1.687	0.425	6.806
11	697.1	528.7	168.4	380	1.391	0.892	0.129	4.949	1.716	0.443	7.293
12	703.0	527.4	175.6	380	1.388	0.903	0.127	5.016	1.707	0.462	7.162
13	704.3	521.1	183.2	380	1.371	0.904	0.133	5.023	1.736	0.482	6.817
14	708.2	517.1	191.1	380	1.361	0.971	0.140	5.468	1.770	0.503	7.354
15	719.3	519.9	199.4	380	1.368	0.978	0.146	5.518	1.799	0.525	7.088
$\bar{x}$					**1.394**				**1.660**		**7.220**
s					**0.016**				**0.078**		**0.203**

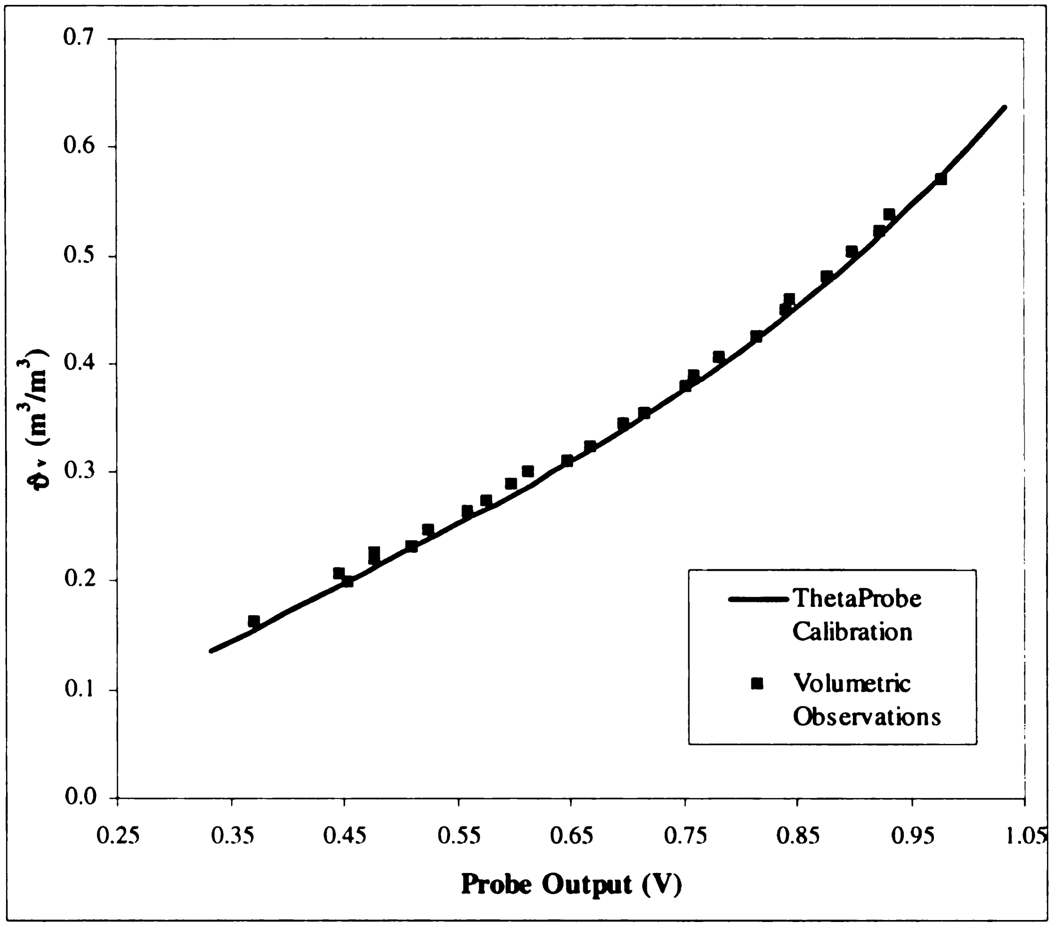

Figure 28. Observed and predicted (via ThetaProbe voltage observations and conversion equations) soil water content for samples collected from a) Corn / no-tillage, b) Soybeans / no-tillage, c) Soybeans / pre-tillage, d) Soybeans / post-tillage, e) Corn / pre-tillage, f) Corn / post-tillage, and g) Forested Conditions.

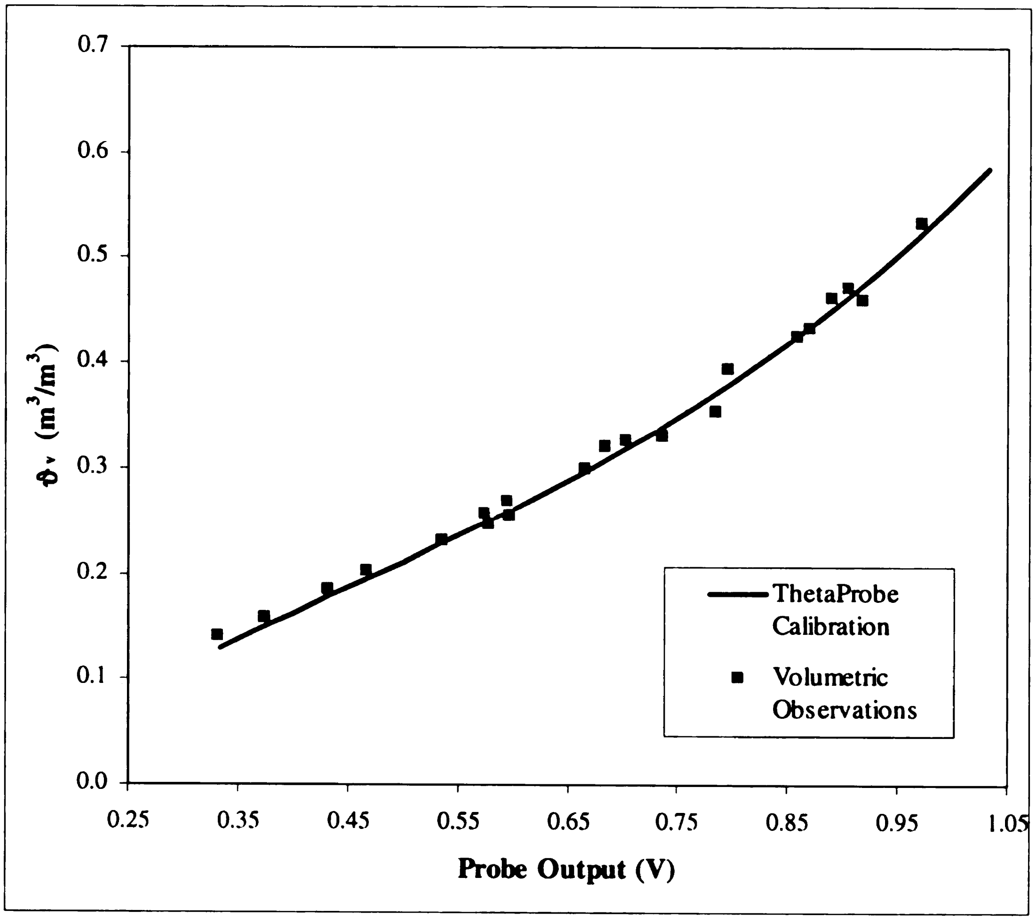
0.7
0.6
0.5
0.4
0.3
0.2
0.1
0.0
ϑv (m³/m³)
0.25
0.35
0.45
0.55
0.65
0.75
0.85
0.95
1.05
Probe Output (V)
ThetaProbe Calibration
Volumetric Observations

Figure 28b.

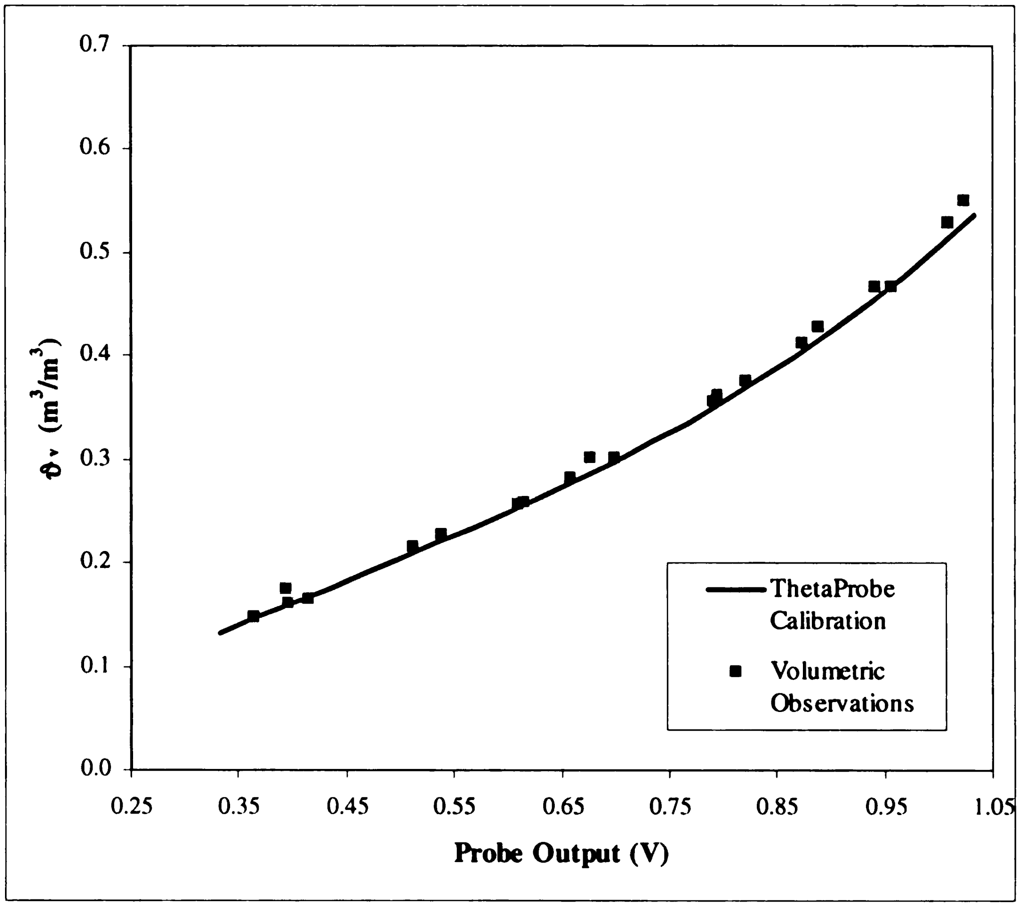

0.7
0.6
0.5
0.4
0.3
0.2
0.1
0.0
ϑ_v (m³/m³)
0.25
0.35
0.45
0.55
0.65
0.75
0.85
0.95
1.05
Probe Output (V)
ThetaProbe Calibration
Volumetric Observations

Figure 28c.

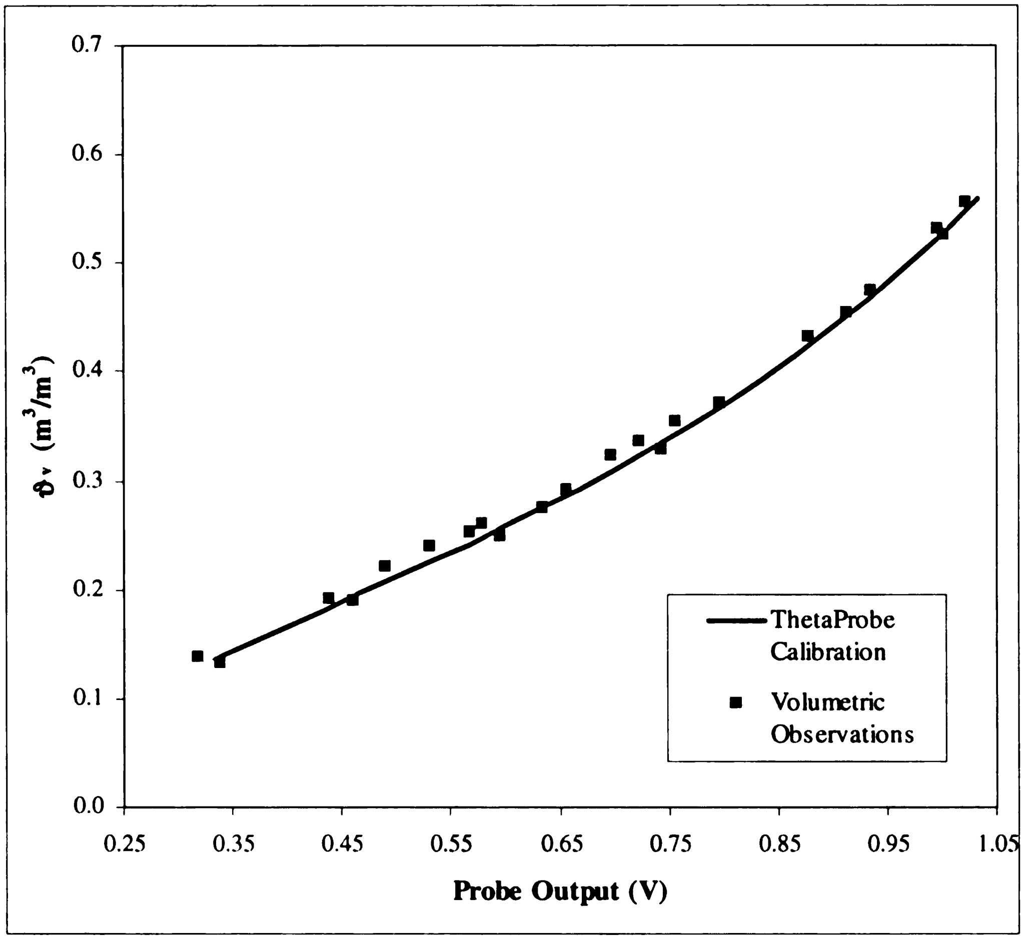
0.7
0.6
0.5
0.4
0.3
0.2
0.1
0.0
ϑv (m3/m3)
0.25
0.35
0.45
0.55
0.65
0.75
0.85
0.95
1.05
Probe Output (V)
ThetaProbe Calibration
Volumetric Observations

Figure 28d.

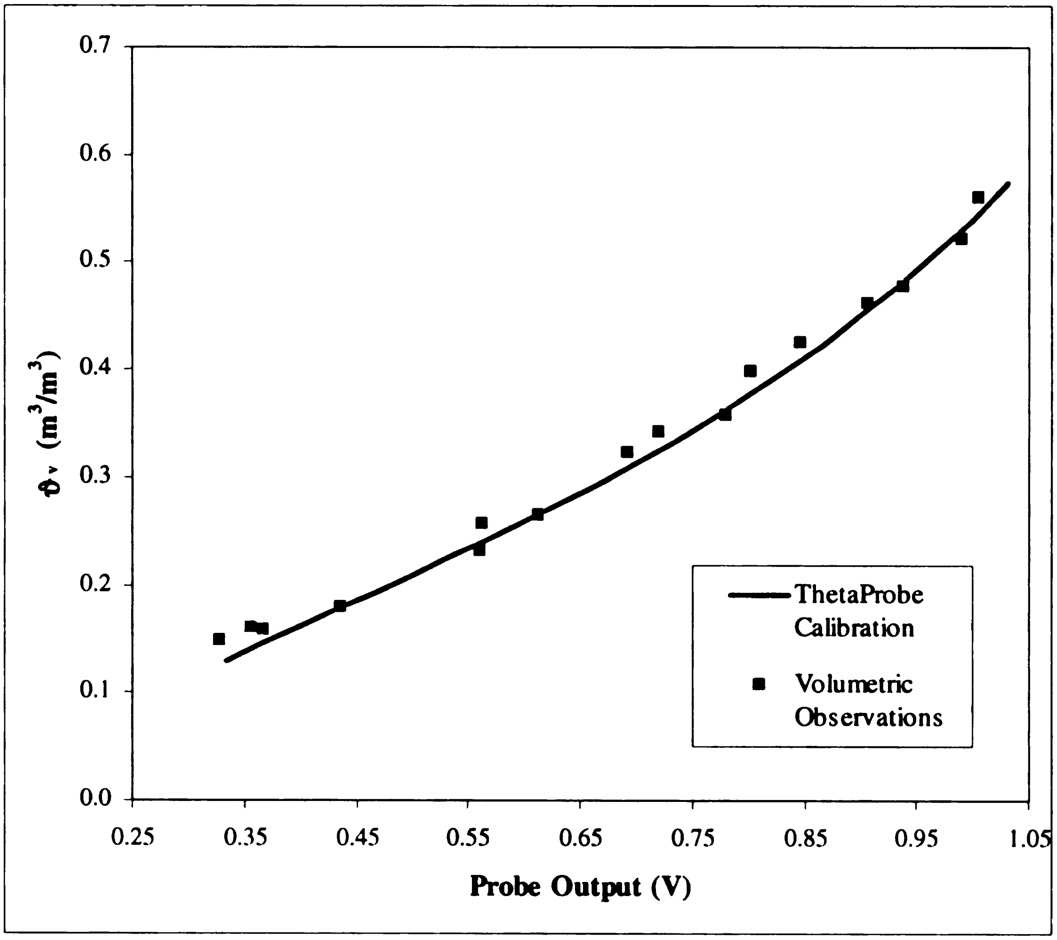
0.7
0.6
0.5
0.4
0.3
0.2
0.1
0.0
ϑ_v (m^3/m^3)
0.25
0.35
0.45
0.55
0.65
0.75
0.85
0.95
1.05
Probe Output (V)
ThetaProbe Calibration
Volumetric Observations

Figure 28e.

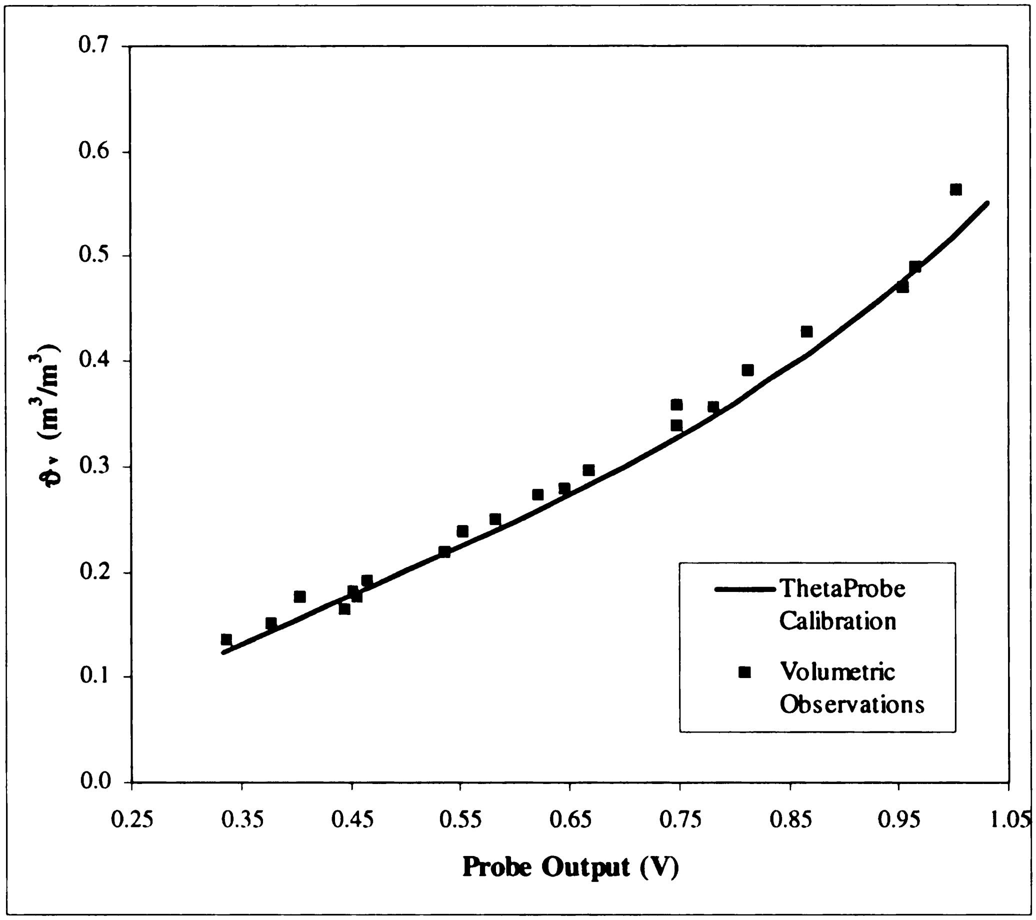

0.7
0.6
0.5
0.4
0.3
0.2
0.1
0.0
ϑv (m3/m3)
0.25
0.35
0.45
0.55
0.65
0.75
0.85
0.95
1.05
Probe Output (V)
ThetaProbe Calibration
Volumetric Observations

Figure 28f.

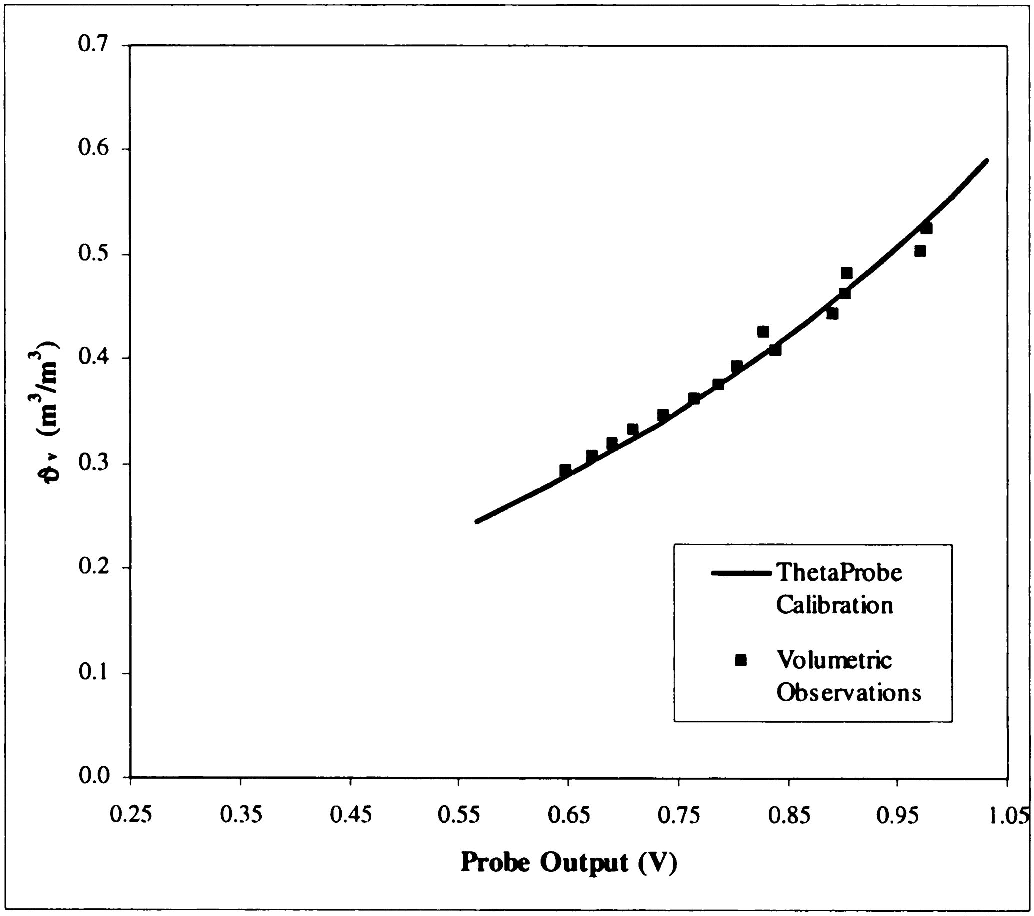
0.7
0.6
0.5
0.4
0.3
0.2
0.1
0.0
ϑ_v (m^3/m^3)
0.25
0.35
0.45
0.55
0.65
0.75
0.85
0.95
1.05
Probe Output (V)
ThetaProbe Calibration
Volumetric Observations

Figure 28g.

APPENDIX C

Computational issues associated to Topographic Wetness Index calculations

In the TAPESG processing of DEM/P and DEM/T a 5,000 m^2 threshold was used as cross-grading area. This threshold was assessed from field observations as necessary acreage to permit channel initialization. For grid cells having calculated A_s contributing area below this threshold, the DEMON flow routing algorithm was used. For all other cells, assumed to be (at least a portion of them) members of the drainage network, and thus unlikely to feature flow dispersion, the D8 algorithm was used to calculate flow direction.

Local slope ($tan\beta$) was estimated with the finite difference algorithm which is reported being superior compared to other gradient calculating algorithms (Skidmore, 1989).

Information on ephemeral flow paths from past intense rainfalls, identified in the field and georeferenced with GPS, was used to improve the accuracy of the estimated flow direction.

The A_s calculated with the DEMON/D8 combination in TAPESG, after being converted to raster files, were used to develop ζ for DEM/P and DEM/T using the $\zeta = ln(A_s / tan\beta)$ relationship in the ArcInfo GRID environment. DYNWETG, used to produce δ, calculates A_e using the D8 algorithm. Thus we expected discrepancies between

ζ and δ calculated for very large drainage times, especially for locations above the channel initialization zone.

Small soil saturated hydraulic conductivity values and very gentle slopes in the sampling area determined τ (100 - 1,000,000 hours) for the δ simulations. For $\tau < 100$ hours, the associated A_e is very small and the index becomes negative, while for more than 1,000,000 hours, δ values reach their asymptote for all grid-cells in the sampling area. The resolution of τ simulated within the specified range, was chosen to increase progressively from the lower to the upper tail of the range because δ is a natural logarithm based index and the influence of one τ unit change on the index value decreases as τ expands. A total of 124 τs (123 in the range mentioned plus ζ where τ is infinite) for each of the two DEMs and uniform/distributed soil property information were used in the analysis, for a total of 496 simulations.

Pixel thinning was evaluated as an alternative to the 3x3 pixel low-pass filter applied to the gridded δ simulation outputs, because it does not result in grid smoothing. The pixel thinning approach however, produced irregular soil water content patterns, which were most obvious for cells on, or in the close proximity of, the drainage network.

The DYNWETG-based simulation output conversion and rasterization, and the value per sampling plot extraction were performed via an ARCINFO Macro Language (AML) script (Table 16).

Table 16. AML script for automating TWI calculation, output conversion and rasterization, and sampling plot index value extraction.

```
/* The "us" prefix in all the file/coverage stands for "Uniform Soil Attributes" and
/* the "vs" for "Distributed (Variable) Soils Attributes"
/*
/* AML requires the following files:
/* afdem.asd          TAPESG DEM/P output file in binary format
/*                    (253 rows x 152 cols, 10 meter resolution)
/*                    OR
/* dlgdem.asd         TAPESG DEM/T output file in binary format
/*                    (827 rows x 313 cols, 10 meter resolution)
/* plotlut.dat        info lookup table for converting the NorthWest to SouthEast plot
/*                    numbering sequence to the field plot number
/* outfloat           Floating point grid (253 * 152) w/ value = 1 for the cell
/*                    containing a plot and "nodata" for all the other cells
/* joinfile.dat       An info table, blank in the beginning of each simulation, where
/*                    index values per plot and simulation are recorded
/* projection_dem     An empty grid file containing projection information (UTM,
/*                    NAD27, Zone 16, Units Meters)
/* drainage_time.txt  A text file with drainage times used in the simulations
/*
/* ------------------------------------

/* Set the Drainage Time text file as variable
   &sv drainage_time = drainage_time.txt

/* Open the Drainage Times File
   &sv amlunit = [open %drainage_time% openstat -READ]

/* Read from the Drainage Times File
   &do &while %openstat% = 0

   &sv num = [read %amlunit% readstat]

/* Create and close the Temporary file to be used in the DYNWETG commmand

   &sv unit = [open vs_temp.txt openstat -write]
   &sv writestat = [write %unit% vs%num%.dwt]
   &sv writestat = [write %unit% Y]
   &sv writestat = [write %unit% afdem.asd]
   &sv closestat = [close %unit%]
```

Table 16 (cont'd).

```
/* Run the DYNWETG program using the parameters specified in the Temporary
/* File created above

   dynwetg < vs_temp.txt

/* Erases the Temporary File

   &sv delstat = [DELETE dwt_temp.txt]

/* Exports the DYNWETG output to ARCINFO format and then converts it to grid
/* Also deals with the "Flipping" problem and defines the projection

   tapestoarc -I vs%num%.dwt -n 4 -A
   asciigrid vs%num%_4.asc vs%num% float
   grid
   vsfl%num% = flip ( vs%num%)
   q
   projectcopy grid projection_dem grid vsfl%num%

/* Calculates a 9-cell-neighbor average for each cell of the wetness grid
   grid
   vsfc%num% = focalmean( vsfl%num%, rectangle, 3, 3 )
   q

/* Removes all intermediate files/coverages except the vsfc%num% ones

           &sys rm vs%num%_4.asc
   &sys rm vs%num%.dwt
   kill vs%num% all
   kill vsfl%num% all

/* Routine for extracting the wetness value per plot

   grid
   out%num% = vsfc%num% * outfloat
   q
   gridpoint out%num% wp%num% dyn_wet
   additem wp%num%.pat wp%num%.pat n1 4 5 b
   additem wp%num%.pat wp%num%.pat t%num% 8 12 F 3
   tables
   select wp%num%.pat
   calculate n1 = wp%num%-id
   calculate t%num% = dyn_wet
   joinitem wp%num%.pat plotlut.dat wp%num%.pat n1 n1
```

Table 16 (cont'd).

```
    q

    dropitem wp%num%.pat wp%num%.pat wp%num%#
    dropitem wp%num%.pat wp%num%.pat wp%num%-id
    infodbase wp%num%.pat t%num%.dbf
    dbaseinfo t%num%.dbf t%num%.dat
    &sys rm t%num%.dbf
    items t%num%.dat
    dropitem t%num%.dat t%num%.dat area
    dropitem t%num%.dat t%num%.dat perimeter
    dropitem t%num%.dat t%num%.dat n1
    joinitem joinfile.dat t%num%.dat joinfile.dat n2 n2
    infodbase t%num%.dat %num%.dbf

    tables
    select t%num%.dat
    erase t%num%.dat
    Y
    Q

    Kill out%num% all
    Kill wp%num% all
    Kill vsfc%num% all

/*  Exports results to a DBASE ver IV format file

    infodbase joinfile.dat af_vs_fc.dbf

    &end

    clear

    &type - - - - - - - - - - - - - - - - - - - - - - - - - - - - - - - - - - - - -
    &type DYNWETG SIMULATION RESULTS FOR EACH PLOT LOCATION
    &type WHERE SUCCESSFULLY GENERATED (IN .DBF FORMAT)
    &type (GROUPED BY DRAINAGE TIME)
    &type - - - - - - - - - - - - - - - - - - - - - - - - - - - - - - - - - - - - -
    &sv closestat = [close -ALL]

    &return

/*  Created by Demetrios Gatziolis, MSU Dept.of Forestry, 1998.
```

REFERENCES

REFERENCES

Ahuja, L.R., O. Wendroth, and D.R. Nielsen. 1993. Relationship between initial drainage of surface soil and average profile saturated conductivity. Soil Sci. Soc. Am. J. 57:19-25.

Band, L.E. 1989. A terrain-based watershed information system. Hydrol. Proc., 3, 151-162.

Barling, R.D., I.D. Moore, and R.B. Grayson. 1994. A quasi-dynamic wetness index for characterizing the spatial distribution of zones of surface saturation and soil water content. Water Resources Research, 30(4): 1029-1044.

Beasley, D.B. 1986. Distributed parameters hydrologic and water quality modeling, in Agricultural Nonpoint Source Pollution: Model Selection and Application, A. Giorgini and F. Zingales, eds., Elsevier, Amsterdam.

Beven K.J. and Kirkby M.J. 1979. A physically based variable contributing area model of basin hydrology. Hydrol. Sci. Bull., 24, 43-69.

Bitelli, G., A. Carrara, M.S. De Torres Curth, and G. Folloni. 1993. Topographical database for EFEDA GIS, Echival Field Experiment in a Desertification-Threatened Area. Annex to Final Report, FU Berlin, Berlin.

Brown D.G., L. Bian, and S.J. Walsh. 1993. Response of a distributed watershed model to variations in input data aggregation levels. Computers and Geosciences, 19(4):499-509.

Burt, T.P. and D.P. Butcher. 1986. Development of topographic indices for use in semi-distributed hillslope runoff models. Geomorphology and land management. Slaymaker O., and D. Balteanu (eds) pp. 1-19. Gebruder Borntraerger, Berlin.

Campbell, C.M., and D.D. Fritton 1994. Factors affecting field-saturated hydraulic conductivity measured by the borehole permeameter technique. J. Soil Science Society of America. 58:1354-1357.

Carrara, A., G. Bitelli, and R. Carla. 1997. Comparison of techniques for generating digital terrain models from contour lines. Int. J. Geographical Information Science, 11(5):541-473.

Costa-Cabral, M.C., and S. Burges. 1994. Digital elevation model networks (DEMON): A model of flow over hillslopes for computation of contributing and dispersal areas. Water Resources Research, 30(6): 1681-1692.

De Roo, A.P.J., L. Hazelhoff, and P.A. Burrough, 1989. Soil erosion modelling using ANSWERS and geographical informations systems. Earth Surface Processes and Landforms, 14:517-532.

Dietrich, W.E., C.J. Wilson, D.R. Montgomery, and J. McKean. 1993. Analysis of erosion thresholds, channel networks, and landscape morphology using a digital terrain model. J. Geology, 101(2), 259-278.

Donigian, A.S. and H.H. Davis. 1978. User's Manual for Agricultural Runoff Management (ARM) Model, EPA 600/3-78-080, U.S. Environmental Protection Agency, Athens GA.

Dorsey, J.D., A.D. Ward, N.R. Fausey, and E.S. Bair. 1990. A comparison of four field methods for measuring saturated hydraulic conductivity. Transactions of the ASAE 33:1925-1931.

Environmental Systems Research Institute (ESRI). 1997. Arc/Info ver. 7.1.2. 380 New York Street, Redlands, CA 92373-8100.

Eklundh, L. and V. Martensson. 1995. Rapid generation of digital elevation models from topographic maps. International Journal of Geographic Information Systems, 9, 329-340.

Fairfield, J., and P. Leymarie. 1991. Drainage networks from grid digital elevation models. Water Resources Research, 27(5):709-717.

Famiglietti, J.S., and E.F. Wood. 1995. Effects of spatial variability and scale on areally averaged evapotranspiration. Water Resources Research, 31(3):649-712.

Foth, H.D. 1984. Fundementals of Soil Science, 7th edition. John Wiley and Sons, New York.

Fried, J.S., D.G. Brown, M.O. Zweifler, and M.A. Gold. 1999. Mapping Contributing Areas for Stormwater Discharge to Streams Using Terrain Analysis (Chapter 7). In Wilson, J.P. and J.C. Gallant (eds) Terrain Analysis: Principles and Applications. Cambridge, Geoinformation International.

Gao, J. 1997. Resolution and accuracy of terrain representation by grid DEMs at a micro-scale. Int. J. Geographical Information Science, 11(2):199-212.

Goodchild, M.F., L.T. Steyaert, B.O. Parks, M.P. Crane, C.A. Johnston, C.A. Maidment, and S Glendinning, eds. 1996. GIS and Environmental Modeling: Progress and Research Issues. Fort Collins: GIS World Inc.

Hammer, R.D., F.J. Young, N.C. Wollenhaupt, T.L. Barney, and T.W.Haitcoate. 1995. Soil Sci. Soc. Am.J., 59:509-519.

Hillel, D. 1971. Soil and Water: Physical principles and processes. Academic Press, New York and London, 288pp.

Horton, R.E. 1933. The role of infiltration in the hydrological cycle. Trans. Am. Geophys. Union, 14, 446-460.

Hutchinson, M.F. 1989. A new procedure for gridding elevation and stream line data with automatic removal of spurious sinks. J. of Hydrology, 106, 211-232.

Iorgulescu, I., and J.P. Jordan. 1994. Validation of TOPMODEL on a small Swiss catchment. J. of Hydrology, 159:255-273.

Knisel, W.G. 1980. CREAMS: A Field Scale Model for Chemicals, Runoff, and Erosion from Agricultural Management Systems, Conservation Research Rep. No 26, U.S. Department of Agriculture, Washington DC.

Kolbl, O., editor. 1996. Application of digital photogrammetric workstations. Proceedings OEEPE Workshop, Lausanne 4-6 March 1996.

Krzystek, P., and F. Ackermann. 1995. New investigations into the practical performance of automatic DEM generation. Proceedings of the ACSM/ASPRS Annual Conference, American Society for Photogrammetry and Remote Sensing and the American Congress on Surveying and Mapping. Bethesda MD. Pp 372-390.

Laflen, J.M., L.J. Lane, and G.R. Foster. 1991. WEPP - A new generation of erosion prediction technology, J. Soil Water Conserv., 46(1):34-38.

McClave, J.T., and P.G. Benson. Statistics for business and economics. 5th edition. Macmillan Publishing Company. 1991. 958 pp.

Mohanty, B.P. Kanwar, R.S. Everts, C.J. 1994. Comparison of saturated hydraulic conductivity measurement methods for a glacial-till soil. J. Soil Science Society of America, 58:672-677.

Moore, I.D., G.J. Burch, D.H. Mackenzie. 1988. Topographic effects on the distribution of surface soil water and the location of ephemeral gullies. Transactions of the ASAE. St. Joseph, Mich. American Society of Agricultural Engineers, 31: 1098-1107

Moore, I.D., R.G. Grayson, and A.R. Larson. 1991. Digital terrain modeling. A review of hydrological, geomorphological and biological applications. Hydrological Processes 5:3-30

Moore, I.D., A. Lewis, and J.C. Gallant. 1993. Terrain attributes: Estimation models and scale effects. Jakeman, A. J., M. B. Beck, and M. McAller, eds, Modeling change in environmental systems. New York: John Wiley and Sons. pp 189-214.

Moore, I.D., and J.C. Gallant. 1997. Terrain analysis programs for the Environmental Sciences - Grid version. Version 6.3. Centre for Resource and Environmental Studies. The Australian National University, Camberra, ACT 0200, Australia.

Muller-Wohlfeil, D.I., W. Lahmer, and V. Krysanova. 1996. Topography based Hydrological Modeling in the Elbe Drainage Basin. Proceedings of the Third International Conference/Workshop on the integration of GIS and Environmental Modeling, Santa Fe, New Mexico.

Novotny and Olem. 1994. Water quality, Prevention, identification, and management of diffuse pollution. V. N. Reinhold Ed. 513pp.

O'Callaghan, J.F., and D.M. Mark. 1984. The extraction of drainage networks from digital elevation data. Computer Vision, Graphics and Image Processing. 28:323-344

O'Loughlin, E.M. 1986. Prediction of surface saturation zones in natural catchments by topographic analysis. Water Resources Research. 22(5) 794-804.

Quinn, P.F., K.J Beven, P. Chevallier, and O. Planchon. 1991. The prediction of hillslope flow paths for distributed hydrological modeling using digital terrain models. J. Hydrol. Process, 5, 59-79.

Quinn, P.F., K.J. Beven, and R. Lamb. 1995. The ln(a / tanb) index: how to calculate it and how to use it within the TOPMODEL framework. Hydrological Processes, 9:161-182.

Skidmore, A.K. 1989 .A comparison of techniques for calculating gradient and aspect fom a gridded digital elevation model. Int. J. of Geographic Information Systems, 3:323-334.

Soil Conservation Service and Michigan Agriculture Experiment Station. Soil Survey of Ingham County, Michigan. August 1979.

SPSS Inc. 1997. SPSS for Windows, standard version. Release 8.0.0.

Troch, P.A., M. Mancini, C. Paniconi, and E.F. Wood. 1993. Evaluation of a distributed catchment scale water balance model. Water Resources Research, 29(6):1805-1817.

U.S. Department of Agriculture. 1994. State soil geographic (STATSGO) data base--data use information, miscellaneous publication number 1492 (rev. ed.): Fort Worth, Texas, Natural Resources Conservation Service.

U.S. Environmental Protection Agency. 1984. Report to Congress: Nonpoint Source Pollution in the U.S. Water Planning Division, U.S. EPA, Washington D.C.

Vertessy, R.A., C.J. Wilson, D.M. Silburn, R.D. Connolly, and C.A. Ciesiolka. 1990. Predicting erosion hazard areas using digital terrain analysis. IAHS AISH Publ., 192, 298-308.

Vieira, S.R., D.R. Nielsen, J.W. Biggar. 1981. Spatial variability of field-measured infiltration rate Soil properties, soil classification. Soil Science Society of America journal. 45 (6) 1040-1048.

Vieux, B.E. 1993. DEM aggregation and Smoothing Effects on Surface Runoff Modeling. J. Computing Civil Engineering. 7(3) 310-338.

Wilson, J.P. 1996. Spatial models of land use systems and soil erosion: The role of GIS. Wegener, M., and Fotheringham, A. S. eds., GIS and Spatial Models: New potential for New Models? London, Taylor and Francis.

Whalley, W.R, 1993. Considerations on the use of time-domain reflectometry (TDR) for measuring soil moisture content. J. Soil Sci., 44 1-9.

White, I., J.H. Knight, S.J Zegelin, and G.C Topp. 1994. Comments on 'Considerations on the use of time-domain reflectometry (TDR) for measuring soil water content' by W. R. Whalley. J Soil Sci.,45 503-508.

Wolock, D.M. 1995. Effects of subbasin size on topographic characteristics and simulated flow paths in Sleepers River watershed, Vermont. Water Resources Research 31(8):1989-1997.

Yeakley, J.A., G.M. Hornberger, W.T. Swank, P.V. Bolstad, and J.M.Vose. 1999. Soil moisture modeling in humid mountainous landscapes. In Wilson, J.P. and J.C. Gallant (eds) Terrain Analysis: Principles and Applications. Cambridge, Geoinformation International.

Young, R.A., et al. 1986. Agricultural Nonpoint Source Pollution Model: A Watershed Analysis Tool, Agricultural Research Service, U.S. Department of Agriculture, Morris, MN.

Zhang, W., and D. R. Montgomery. 1994. Digital elevation model grid size, landscape representation, and hydrologic simulations. Water Resources Research 30(4):1019-1028.

MICHIGAN STATE UNIV. LIBRARIES
31293017879945